HHS Public Access

Author manuscript

Nature. Author manuscript; available in PMC 2024 June 07.

Published in final edited form as:

Nature. 2023 June ; 618(7967): 1006–1016. doi:10.1038/s41586-023-06147-9.

Antagonistic circuits mediating Infanticide and Maternal Care in Female Mice

Long Mei[1], **Rongzhen Yan**[1,4], **Luping Yin**[1,4], **Regina Sullivan**[2], **Dayu Lin**[1,3]

[1]Neuroscience Institute, New York University Langone Medical Center, New York, NY, USA

[2]Emotional Brain Institute, Nathan Kline Institute, Child and Adolescent Psychiatry, New York University Langone Medical Center, New York, NY USA

[3]Department of Psychiatry, New York University Langone Medical Center, New York, NY, USA; Center for Neural Science, New York University, New York, NY, USA

Summary

In many species, including mice, females show strikingly different pup-directed behaviors based on their reproductive state[1,2]. Naïve wild female mice often kill pups, while lactating females are dedicated to pup caring[3,4]. The neural mechanisms that mediate infanticide and its switch to maternal behaviors during motherhood remain unclear. Here, based on the hypothesis that maternal and infanticidal behaviors are supported by distinct and competing neural circuits[5,6], we used the medial preoptic area (MPOA), a key site for maternal behaviors[7–11], as a starting point and identified three MPOA-connected brain regions that drive differential negative pup-directed behaviors. Further functional manipulation and *in vivo* recording revealed that estrogen receptor alpha (Esr1) expressing cells in the principal nucleus of the bed nucleus of stria terminalis (BNSTpr^{Esr1}) are necessary, sufficient, and naturally activated during infanticide in female mice. MPOA^{Esr1} and BNSTpr^{Esr1} neurons form reciprocal inhibition to control the balance between positive and negative infant-directed behaviors. During motherhood, MPOA^{Esr1} and BNSTpr^{Esr1} cells change their excitability in opposite directions, supporting a drastic switch of female behaviors towards the young.

Correspondences: Long.Mei@nyulangone.org and Dayu.Lin@nyulangone.org.

[4]Equal contribution

Author Contribution statement

D.L. and M.L. conceived the project, designed experiments, analyzed data and wrote the paper. D.L. supervised the project. M.L. performed most experiments and prepared figures. R.Y. and L.Y. performed slice recording experiments and prepared related figures. R.S. provided critical feedback on the experiments.

Statement of competing interests

The authors declare no competing interests.

Code Availability

MATALB code used in this study can be downloaded from 10.5281/zenodo.7772552.

Additional Information statement

Supplementary Information is available for this paper. Correspondence and requests for materials should be addressed to dayu.lin@nyulangone.org. Reprints and permissions information is available at www.nature.com/reprints.

Introduction

At birth, the young are vulnerable and powerless for nearly all mammalian species. Its chance of survival critically depends on care and protection from the parents, especially mothers. Consequently, a set of robust and stereotypical maternal behaviors, such as nursing, crouching, grooming and retrieving, have evolved to ensure the needs of the young are met. However, females do not always care for pups. Across a wide range of mammalian species, it is not uncommon for virgin females to show hostile behaviors towards pups of the same species[12,13]. In a survey involving 289 mammalian species, infanticide was found in 31% of species, with a higher percentage in species that breed in groups[12]. Despite the prevalence of infanticide in mammalian females, including mice[3,4], it is rarely studied under laboratory conditions partly because adult females of many inbred strains of mice, e.g., C57BL/6, rarely show such behavior, likely due to inbreeding[14,15]. Female mice of outbred strains, e.g., Rockland-Swiss, appear to have retained more naturalistic behaviors, including a higher level of infanticide than inbred mice, although the exact likelihood varies with age[16].

The neural circuit of maternal behaviors has been extensively studied, and the medial preoptic area (MPOA) has been firmly established as a critical region for maternal behaviors[7–11]. Recent studies further revealed MPOA cells expressing estrogen receptor alpha ($MPOA^{Esr1}$)[17,18] or galanin[19,20] as the key populations to facilitates maternal behaviors, such as pup retrieval and grooming. Interestingly, MPOA cells relevant for parental behaviors are mainly inhibitory[18,19,21]. In fact, activating GABAergic cells in the MPOA is sufficient to elicit pup retrieval and nest building[22] whereas activating MPOA glutamatergic cells elicits anxiety-like behaviors[23].

In contrast to our extensive knowledge of the maternal circuit, little is known regarding the neural substrates responsible for infanticide in females. A few recent studies started to reveal neural substrates relevant for infanticide in males. Lesioning rhomboid nucleus of the bed nucleus of stria terminalis (BNSTrh)[24] or inactivating urocortin-3 cells in perifornical area[25] reduced pup attack, whereas activating amygdalohippocampal area[26] or GABAergic cells in the medial amygdala posterodorsal part (MeApd)[27] promoted pup attack in males. However, the roles of these regions in female infanticide are either minimal or unexplored[24–27].

Given that maternal behavior-relevant cells in the MPOA are mainly inhibitory and brain lesions that impair parental behaviors sometimes increase infanticide and *vice versa*[19,24,25,28,29], it was hypothesized that the maternal care circuit and infanticide circuit might counteract each other through reciprocally inhibition[2,5]. Based on this hypothesis, we systematically manipulated regions directly connected with MPOA and identified multiple brain areas that robustly promote negative pup-directed behaviors in female mice. We further examined one of the regions, the principal nucleus of the bed nucleus of stria terminalis (BNSTpr) in detail, and identified the estrogen receptor alpha (Esr1) expressing cells in the BNSTpr ($BNSTpr^{Esr1}$) as indispensable for infanticide in female mice.

Main

Regions promoting female infanticide—If the neural circuits driving infanticide and maternal behaviors antagonize each other, reducing the activity in maternal circuit should

favor the activation of the infanticide circuit. To test this hypothesis, we ablated MPOA^{Esr1} neurons and found that the manipulation caused 7/8 virgin non-infanticidal females to attack pups without altering pup investigation (Extended Data Fig. 1a–g). Furthermore, we chemogenetically inhibited MPOA^{Esr1} neurons using hM4Di and observed qualitatively similar results: while no animal attacked pups after saline injection, all hM4Di, but no mCherry females, showed infanticide after CNO injection (Extended Data Fig. 1h–n). These results support the hypothesis that MPOA plays an important role in antagonizing infanticide.

We next aimed to identify MPOA-connecting regions that are activated during infanticide. To achieve this goal, we first searched for female mice that express infanticide spontaneously. As previously reported, infanticide is rare in adult C57BL/6 females[14,15,30]: only 2 out of 165 virgin C57BL/6 female mice attacked pups in our study. In contrast, approximately one-third (50/146) of virgin Swiss Webster (SW) females attacked and killed pups, making SW mice a suitable animal model for studying the female infanticide circuit in the lab.

Next, We identified regions upstream or downstream of MPOA by injecting high titer (>1 × 10^{13}) AAV1-Syn-Cre[31] into MPOA of Ai6[32] SW female mice (Extended Data Fig. 2a). MPOA-connecting cells were widely distributed in the brain, including 18 regions containing more than 1% of total labeled cells (Extended Data Fig. 2b–d). Half (9/18) of the highly connected regions were within the hypothalamus and collectively contributed to 69% of total labeled cells (Extended Data Fig. 2d). Outside of the hypothalamus, the densely labeled cells were found in the lateral septum (LS), nucleus accumbens (NAc), paraventricular thalamus (PVT), BNSTpr, MeApd, posterior amygdala (PA), ventral subiculum (SUBv), ventral tegmental area (VTA) and periaqueductal gray (PAG) (Extended Data Fig. 2d).

BNSTpr, PVT, and MeApd showed a significantly higher number of c-Fos positive cells in females after infanticide than in single-housed undisturbed females (Fig. 1a–b). When we considered only MPOA-connecting cells (tracer+), infanticide significantly increased c-Fos expression in LS, BNSTpr, PVT, paraventricular nucleus (PVN), ventrolateral part of the ventromedial hypothalamus (VMHvl), MeApd, PA, and supramammillary nucleus (SUM) tracer+ cells (Fig. 1c), although c-Fos expression in the LS, PVN and PA tracer+ cells was even high after maternal behaviors (Extended Data Fig. 2e–i). Based on the c-Fos expression pattern and MPOA connectivity, we decided to chemogenetically activate MPOA-connecting cells in the BNSTpr, MeApd, VMHvl, PVN, PVT, and SUM during pup interaction. We also included ventral premammillary nucleus (PMv) in our manipulation list, given its function in inter-male aggression[33,34]. As we aimed at identifying regions that enhance infanticide, we used C57BL/6 female mice for this experiment given their near zero spontaneous infanticide.

Strikingly, pharmacogenetic activation of MPOA-connecting BNSTpr (BNSTpr^{MPOA}) or MeApd (MeApd^{MPOA}) cells elicited repeated attack towards pups in the majority of tested C57BL/6 females (Fig. 1d–h, k, l–n and q), while the total duration of pup investigation did not change (Fig. 1i and o). Activating the MeApd^{MPOA} cells, but not BNSTpr^{MPOA}

cells, also increased pup grooming (Fig. 1j and p), a behavioral change that was observed previously during optogenetic activation of MeApd GABAergic cells[27]. Animals that expressed mCherry in MeApd^{MPOA} or BNSTpr^{MPOA} cells showed no infanticide after either saline or CNO injection (Fig. 1f–q).

When the MPOA-connecting VMHvl (VMHvl^{MPOA}) cells were chemogenetically activated, the test females avoided the pups, but none showed infanticide (Extended Data Fig. 3a–c). When the MPOA-connecting SUM cells were activated, pup grooming decreased slightly while other behaviors did not change significantly (Extended Data Fig. 4d). Activating MPOA-connecting PVT, PVN, and PMv cells caused no significant behavior change towards the pups (Extended Data Fig. 4e–g). These results suggest that pup-directed behaviors, including pup avoidance, pup grooming, and infanticide, are mediated by different combinations of brain regions. BNSTpr^{MPOA} cells could play an important and specific role in driving infanticide.

BNSTpr^{MPOA} activation drives infanticide—To understand whether the BNSTpr^{MPOA} cells drive infanticide acutely or only increase the likelihood of its expression, we optogenetically activated BNSTpr^{MPOA} cells bilaterally in virgin C57BL/6 female mice (Extended Data Fig. 4a–c). Upon light stimulation (20 ms, 20 Hz, 20 s) at even the lowest intensity (0.5 mW), 10/11 ChR2-expressing females atteked pup after contact in approximately 65% of trials, while no GFP-expressing females attacked the pups (Extended Data Fig. 4d–i). The increase in attack probability was almost immediate after light onset and the average latency to attack was approximately 3 s (Extended Data Fig. 4g, j). Increasing light intensity did not change the induced behavior qualitatively, although there was a trend of decrease in light-evoked attack probability (Extended Data Fig. 4d–j).

Stress can negatively impact maternal behaviors[35,36], and several BNST subdivisions (though not BNSTpr) were shown to modulate stress and anxiety[37–39]. To understand whether BNSTpr^{MPOA} stimulation-evoked infanticide is due to an increase in anxiety, we examined light-evoked behavioral changes in a real-time place preference test (RTPP) and an elevated plus maze test (EPM) (Extended Data Fig. 4k–n). We found that activation of BNSTpr^{MPOA} increased the fraction of time spent on the stimulated side (Extended Data Fig. 4l) and open arms (Extended Data Fig. 4n), suggesting that BNSTpr^{MPOA} stimulation is not aversive or anxiogenic. Thus, the stimulation-induced infanticide is not secondary to an increase in stress.

BNSTpr^{Esr1} activation drives infanticide—Esr1 expresses widely in regions important for social behaviors[40]. Esr1 positive cells in the VMHvl, MPOA, and PA were found preferentially involved in social behaviors compared to Esr1 negative cells[18,41–43]. Within the BNST, Esr1 is concentrated in the BNSTpr. Its expression is lower in males than females regardless of the female's reproductive state (Extended Data Fig. 5a–c)[44]. Thus, we next investigated the possibility that Esr1 is a relevant molecular marker for infanticide cells in the BNSTpr. Immunostaining revealed that Esr1 expresses in approximately half of the BNSTpr cells (Extended Data Fig. 5d–f). Strikingly, over 90% of infanticide-induced c-Fos cells overlap with Esr1 cells, and approximately 85% of MPOA-connecting BNSTpr cells are Esr1 positive (Extended Data Fig. 5d–f). Within the BNSTpr^{Esr1} cells, approximately

15% express infanticide-induced c-Fos (Extended Data Fig. 5f). Thus, Esr1 preferentially marks the BNSTpr population activated by infanticide and largely encompasses the cells connected with MPOA.

We then optogenetically activated BNSTpr^{Esr1} neurons bilaterally in virgin Esr1-2A-Cre C57BL/6 female mice and found that the manipulation induced pup attack even more reliably and quickly than BNST^{MPOA} cell activation (Fig. 2a–l). Regardless of the light intensity, infanticide was induced in all tested females (8/8) and in 92% of total pup interaction stimulation trials with an average latency of 1s (Fig. 2k–l). No test animals showed spontaneous pup attack without light, and no GFP control animals attacked the pups during the entire test session (Fig. 2d–l). We further asked whether BNSTpr^{Esr1} activation can override the maternal behaviors in mothers. Indeed, light stimulation induced reliable infanticide in all lactating females (6/6), even towards their own pups, while all mothers quickly retrieved and cared for pups with sham stimulation (Fig. 2h–l).

To understand whether the function of BNSTpr^{Esr1} cells is strain-specific, we carried out the optogenetic activation in non-infanticidal Esr1-2A-Cre females with SW background and observed similar results in both virgin and lactating females (Extended Data Fig. 5g–m). These results indicate that BNSTpr^{Esr1} cells are sufficient to drive infanticide in females regardless of animals' reproductive state and genetic background.

BNSTpr^{Esr1} is necessary for infanticide—To determine whether BNSTpr^{Esr1} neurons are necessary for infanticide in female mice, we inhibited BNSTpr^{Esr1} cells using h4MDi in virgin Esr1-2A-Cre SW female mice (Fig. 2m–o). For the 9 spontaneously infanticidal hM4Di female mice, all attacked and killed pups after saline injection, whereas only one did so after CNO injection and 6/9 females even retrieved the pups (Fig. 2p–s). For the 5 h4MDi females that neither attacked nor retrieved pups, 4/5 females retrieved pups after CNO injection while none did do after saline injection (Extended Data Fig. 6a–c). CNO injection did not change the total duration of pup investigation (Extended Data Fig. 6d). Similarly, inactivating BNSTpr^{Esr1} cells in lactating females shortened the latency to retrieve all pups (Extended Data Fig. 6e–h). Altogether, these results support that BNSTpr^{Esr1} cells not only drive infanticide but also suppress maternal behaviors in female mice.

BNSTpr^{Esr1} and MPOA^{Esr1} mutually inhibit—Inhibiting MPOA^{Esr1} cells impairs maternal behavior and promotes infanticide, whereas inhibiting BNSTpr^{Esr1} cells impairs infanticide and promotes maternal behaviors. These results strongly suggest an antagonistic relationship between these two populations, possibly through mutual inhibition. To test this hypothesis, we first examined the projection patterns of BNSTpr^{Esr1} and MPOA^{Esr1} cells by virally expressing GFP in these cells. We found dense terminal fields from BNSTpr^{Esr1} cells in the Esr1-enriched region in the MPOA and vice versa (Fig. 3a–c and f–h). A survey of the GFP fibers throughout the brain revealed that MPOA represents one of the major downstream regions of the BNSTpr^{Esr1,} whereas BNSTpr receives moderate input from MPOA^{Esr1} cells (Figs. 3d–e and i–j).

We then performed ChR2-assisted circuit mapping on brain slices to investigate synaptic connections between MPOA^{Esr1} to BNSTpr^{Esr1} cells (Fig. 3k, s). We found that BNSTpr^{Esr1}

terminal activation evoked inhibitory postsynaptic currents (oIPSCs) in >90% (20/22) of MPOA^{Esr1} neurons, including two neurons showing both oIPSCs and evoked excitatory postsynaptic currents (oEPSCs) (Fig. 3l). The oIPSC was large (Mean ± SEM: 930 ± 166 pA) and monosynaptic as it was blocked by tetrodotoxin (TTX) and rescued by TTX and 4-aminopyridine (4-AP) (Fig. 3m–n). The oIPSC is mediated mainly by $GABA_A$ receptors and to a lesser extent by glycine receptors: $GABA_A$ receptors antagonist, gabazine (SR), completely blocked oIPSC in 56% (20/36) of cells (Fig. 3m–p) and the residual oIPSCs were further blocked by glycine receptor inhibitor Strychnine (Fig. 3q–r).

Similarly, 94% (33/35) BNSTpr^{Esr1} showed oIPSCs upon MPOA^{Esr1} terminal stimulation, including 10 cells that showed both oIPSCs and oEPSCs (Fig. 3t). The higher proportion of cells showing oEPSCs upon MPOA^{Esr1}→ BNSTpr^{Esr1} stimulation in comparison to BNSTpr^{Esr1} → MPOA^{Esr1} stimulation is consistent with the fact that BNSTpr^{Esr1} cells are nearly exclusively GABAergic, whereas approximately a quarter of MPOA^{Esr1} cells are glutamatergic[45,46]. The oIPSCs can be blocked by bath application of TTX and rescued by TTX and 4-AP, suggesting the monosynaptic nature of the connection (Figs. 3u–v). The oIPSCs are mediated mainly by the $GABA_A$ receptor and, to a smaller extent, by the glycine receptor (Figs. 3u–z). These results suggested that BNSTpr^{Esr1} and MPOA^{Esr1} neurons form strong reciprocal inhibitory connections.

MPOA^{Esr1}→BNSTpr suppresses infanticide—We next expressed ArchT in MPOA^{Esr1} cells and optogenetically inhibited the MPOA^{Esr1} terminals in the BNSTpr in virgin non-infanticidal Esr1-2A-Cre SW female mice (Fig. 4a, Extended Data Fig. 7a–b). Slice recording confirmed that yellow light effectively blocked the inhibitory synaptic transmission from ArChT-expressing axon terminals (Extended Data Fig. 8). We found that inhibiting MPOA^{Esr1}–BNSTpr projection significantly increased pup attack (Fig. 4b–4e). Upon light delivery, 5/6 ArchT females attacked pups with a latency of approximately 1 min, typically after a period of pup investigation, while none of the mCherry control animals attacked pups (Fig. 4b–d). Given the long latency of light-induced attack, this result suggests that removing the inhibition from MPOA^{Esr1} to BNSTpr increased the probability of infanticide but did not trigger attack action acutely, as observed during BNSTpr^{Esr1} activation.

Next, we expressed ChrimsonR in MPOA^{Esr1} cells and activated the MPOA^{Esr1} to BNSTpr projection in infanticidal virgin SW females (Fig. 4f). Strikingly, all ChrimsonR females stopped attacking pups, and 3/7 mice showed pup retrieval (Fig. 4g–j). However, histological analysis revealed c-Fos induction in the MPOA after light delivery to BNSTpr, suggesting activation of MPOA^{Esr1} cell body possibly due to backpropagation of action potentials or disinhibition after BNSTpr inhibition (Extended Data Fig. 7c, d, f). To prevent MPOA cell body activation, we co-injected Cre-dependent hM4Di-mCherry and ChR2-EYFP viruses into the MPOA and injected CNO 30 min before optogenetic activation of MPOA^{Esr1}-BSNTpr projection (Fig. 4f). Indeed, CNO effectively eliminated terminal stimulation-induced c-Fos increase in the MPOA (Extended Data Fig. 7c, e, f). Under this condition, light activation of MPOA^{Esr1}–BNSTpr terminals suppressed infanticide but did not increase maternal behaviors (Fig. 4g–j). Thus, MPOA^{Esr1} input to BNSTpr can bi-directionally

modulate infanticidal behavior – an increase in MPOA^{Esr1} input suppresses infanticide while a decrease in input facilitates infanticide.

BNSTpr^{Esr1}→MPOA suppresses maternal care—When we optogenetically inhibited BNSTpr^{Esr1} input to MPOA in spontaneously infanticidal females, we observed behavioral changes opposite to that during MPOA^{Esr1}–BNST pathway inhibition (Fig. 4k–o, Extended Data Fig. 7g–h). While all mCherry control females showed infanticide, only 1/6 ArchT females briefly attacked the pup with light delivery, suggesting that BNSTpr^{Esr1} inhibition onto MPOA is functionally important to ensure the expression of infanticide (Fig. 4k–o).

When we optogenetically activated BNSTpr^{Esr1}–MPOA pathway in non-infanticidal females, maternal behaviors were suppressed, and all females (5/5) attacked the pups repeatedly (Fig. 4p–t). However, BNSTpr^{Esr1}–MPOA terminal stimulation induced strong c-Fos in BNSTpr (Extended Data Fig. 7i, j and l). We thus chemogenetically inhibited BNSTpr^{Esr1} cell bodies while optogenetically activating BNSTpr^{Esr1}–MPOA terminals (Fig. 4p, Extended Data Fig. 10k–l). Under this scenario, we found reduced maternal behaviors but no increase in infanticide, suggesting that BNSTpr^{Esr1}–MPOA pathway mainly plays a role in suppressing maternal behaviors (Fig. 4q–t). Altogether, these results support the hypothesis that BNSTpr^{Esr1} and MPOA^{Esr1} directly antagonize each other through mutual inhibition. The relative activity between these two regions determines the female behaviors towards the pups.

BNSTpr^{Esr1} vs. MPOA^{Esr1} cell responses—Why a pup-killing virgin female suddenly cares for the young after becoming a mother? Our functional results suggest that this behavior switch could be due to a change in the relative activity of BNSTpr^{Esr1} and MPOA^{Esr1} cells. Thus, we next performed longitudinal population Ca^{2+} recordings to reveal potential response changes of BNSTpr^{Esr1} and MPOA^{Esr1} cells during motherhood (Fig. 5a–g). Over 90% GCaMP6f positive cells express Esr1, confirming that the fluorescence signal largely came from Esr1 cells (Fig. 5c).

During the first pup contact after its introduction, we observed a sharp increase in Ca^{2+} signal of BNSTpr^{Esr1} cells in hostile virgin females but not in lactating females (Fig. 5h–i, and m). During subsequent pup approach, Ca^{2+} signal did not significantly increase regardless of the reproductive state of the females (Fig. 5j, n and o). During close pup investigation, Ca^{2+} increased only slightly (Figs. 5k, n and o). When the hostile female attacked a pup, BNSTpr^{Esr1} cell activity increased strongly and maintained at a high level until the end of the attack (Fig. 5h1, l1 and n). In contrast, the cell activity increased only slightly during pup retrieval in mothers (Fig. 5h2, l2 and n). The average response of BNSTpr^{Esr1} cells during infanticide is significantly higher than that during retrieval (Fig. 5o). Overall, BNSTpr^{Esr1} cells showed higher responses to pups in hostile virgins than mothers (Fig. 5m–o). Control animals that expressed GFP in BNSTpr^{Esr1} or MPOA^{Esr1} cells showed no response during any pup-directed behaviors, suggesting the responses of GCaMP6 animals are contributed minimally by movement artifacts (Extended Data Fig. 9a–n). Additionally, BNSTpr^{MOPA} cell responses during pup interaction were found similar to BNSTpr^{Esr1} cell responses (Extended Data Fig. 9o–y).

The response pattern of MPOA^{Esr1} cells is distinct from that of BNSTpr^{Esr1} cells (Fig. 5p–w). The activity increase during pup entry was the highest in mothers and lowest in hostile virgins (Fig. 5p–q and u). In virgin hostile females, MPOA^{Esr1} cell activity increased minimally during approach and investigation and not at all during attacking pups (Fig. 5p1–t1, and v). In maternal virgin females and mothers, Ca^{2+} signal started to rise when the female approached the pup, continued to increase during investigation, and reached maximum during retrieval (Fig. 5p2–t3, and v). The average response of MPOA^{Esr1} cells during retrieval is significantly higher than during infanticide (Fig. 5w).

To directly compare the temporal dynamics of BNSTpr^{Esr1} and MPOA^{Esr1} cells, we recorded Ca^{2+} signals from these two populations simultaneously (Extended Data Fig. 10a–e). During pup approach and investigation, MPOA^{Esr1} cell activity rose earlier than that of BNSTpr^{Esr1} cells in both hostile virgin female and mothers, suggesting higher sensitivity of MPOA^{Esr1} cells to pup cues than BNSTpr^{Esr1} cells (Extended Data Fig. 10f–g). At the onset of pup attack, MPOA^{Esr1} cell activity decreased while BNSTpr^{Esr1} cell activity continuously increased (Extended Data Fig. 10f1–h1). Hence, at the offset of attack, MPOA^{Esr1} cell activity was below baseline, while BNSTpr^{Esr1} cell activity was above baseline (Extended Data Fig. 10g1). In mothers, MPOA^{Esr1} cell was highly active during pup investigation and retrieval, whereas BNSTpr^{Esr1} cell activity stayed low throughout pup-directed behaviors (Extended Data Fig. 10f2–h2). The ratio of overall activity between BNSTpr^{Esr1} and MPOA^{Esr1} cells (BNSTpr^{Esr1}/MPOA^{Esr1}) during pup interaction was >1 in hostile virgins and <1 in mothers (Extended Data Fig. 10i).

C57BL/6 females rarely show infanticide, making it difficult to compare the BNSTpr^{Esr1} and MPOA^{Esr1} cell responses in infanticidal and maternal animals. Nevertheless, c-Fos expression pattern in maternal virgin C57BL/6 females is similar to that of maternal SW females: high in MPOA and low in BNSTpr, which is opposite to the pattern observed in infanticidal SW females (Extended Data Fig. 10j–l). Altogether, these results suggest a reverse in the relative activity level between MPOA^{Esr1} and BNSTpr^{Esr1} cells during motherhood.

Exctability changes during motherhood—What physiological mechanism is responsible for the *in vivo* response change of BNSTpr^{Esr1} and MPOA^{Esr1} cells during motherhood? To address this question, we performed *in vitro* current-clamp recording of MPOA^{Esr1} and BNSTpr^{Esr1} cells from diestrus hostile virgin, diestrus maternal virgin, and lactating (postpartum day 3) SW female mice and found distinct state-dependent changes in MPOA^{Esr1} and BNSTpr^{Esr1} cell excitability (Fig. 6a–e). MPOA^{Esr1} cells in hostile virgin females were prone to depolarization block and did not maintain high spiking activity with a moderate level of current injection (>100pA), whereas MPOA^{Esr1} cells in mothers continued to increase firing with large current injections (Fig. 6a–b). The excitability of MPOA^{Esr1} cells in maternal virgins was between that of hostile virgins and mothers (Fig. 6a–b). In contrast, the excitability of BNSTpr^{Esr1} cells in hostile and maternal virgin females was similar (Fig. 6c–d). However, BNSTpr^{Esr1} cells in mothers were less excitable than those in virgin females, as revealed by the spike frequency – current (F-I) curves (Fig. 6c–d). Between BNSTpr^{Esr1} and MPOA^{Esr1} cells, MPOA^{Esr1} were generally more active, as reflected by their higher maximum action potential (AP) number during current injection,

and this difference was the largest in mothers (Fig. 6e). Overall, MPOA^{Esr1} cells are more excitable in mothers than virgin females, while the opposite is true for BNSTpr^{Esr1} cells. These opposing changes in the excitability of MPOA^{Esr1} and BNSTpr^{Esr1} cells could underlie their reversed *in vivo* response patterns to pups during motherhood.

Lastly, we asked whether the different tendency of SW and C57BL/6 virgin females to infanticide could reside in their differences in BNSTpr^{Esr1} cell properties. We recorded BNSTpr^{Esr1} cells from virgin C57BL/6 females (BNSTpr$^{Esr1.C57)}$ and found that they were much less excitable than those in SW females (BNSTpr$^{Esr1.SW}$) (Fig. 6f–i). Approximately half of BNSTpr$^{Esr1.C57}$ cells (23/44) could fire no more than two spikes regardless of the amount of injected current, whereas the same was true for only 1/57 BNSTpr$^{Esr1.SW}$ cells in virgin females (Fig. 6f–g). The spiking frequency of BNSTpr$^{Esr1.C57}$ cells was significantly lower than that of BNSTpr$^{Esr1.SW}$ cells in virgin females across current steps (Fig. 6h–i). While the excitability of BNSTpr^{Esr1} cells decreased in SW mothers, it did not change in C57 mothers (Fig. 6h–i). These results revealed dampened excitability of BNSTpr^{Esr1} cells in virgin C57BL/6 females, which could contribute to a lack of infanticidal behaviors in these animals.

No effect on maternal aggression—Additionally, we examined BNSTpr^{Esr1} cell responses and functional relevance to adult-directed behaviors (Supplementary Note 1). BNSTpr^{Esr1} and BNSTpr^{MPOA} cells in virgin females also increased activity during adult-directed social behaviors but to a lesser extent than during infanticide. Importantly, BNSTpr^{Esr1} cells responded minimally during maternal aggression and chemogenetic inactivation of BNSTpr^{Esr1} cells did not alter maternal aggression, supporting a specific role of BNSTpr^{Esr1} cells in pup-directed attack. Optogenetic activation of BNSTpr^{Esr1} or BNSTpr^{MPOA} cells rarely induced attack towards adults but did increase social grooming and sometimes male-style mounting in virgin females. Lastly, pathway-specific activation suggested that BNSTpr^{Esr1} optogenetic activation-induced social grooming was not mediated by its projection to MPOA.

Discussion

Though initially considered a rare pathological behavior, infanticide may in fact be an adaptive behavior to increase an individual's reproductive success in both males and females in many species[12,47]. Here, using MPOA as an entry point, we identified BNSTpr^{Esr1} cells as a key population for driving hostile behaviors towards the young in female mice. Both BNSTpr^{Esr1} and MPOA^{Esr1} cells are primarily GABAergic. They form strong reciprocal inhibition to antagonize each other's behavior output. During motherhood, the relative activities between BNSTpr^{Esr1} and MPOA^{Esr1} cells reverse to support the drastic behavioral changes of the females to ensure the survival of the young (Fig. 6j).

Our study also revelaed the infanticide promoting effect of MeApd^{MPOA} cells. Interestingly, while BNSTpr is mainly activated by infanticide and MPOA by maternal care, MeA is activated by both infanticide and maternal behaviors. The potential dual rols of MeA cells in pup-directed behaviors were also suggested by recent functional studies of MeApd GABAergic cells[27]. Importantly, only c-Fos induced by infanticide, but not maternal care,

preferentially overlaps with MeApd^{MPOA} cells, suggesting that infanticide and maternal care could activate distinct MeApd cells that differ in their projection patterns. Consdiering that MeApd cells also project strongly to BNSTpr and the opposing functions of BNSTpr and MPOA in pup-directed behaviors, it is possible that BNSTpr-projecting and MPOA-projecting MeApd cells mediate different pup-directed behaviors. Future circuit studies will help test this hypothesis. Notably, MeA, like BNSTpr and MPOA, are dominated by GABAergic cells, suggesting the antagonism between infanticide and maternal circuits likely occur at multiple levels (Supplementary Note 2).

It is worth noting that BNSTpr^{Esr1} is not a homogenous population. Knoedler et al. recently performed scRNAseq of BNSTpr^{Esr1} cells and identified 36 molecularly distinguishable clusters[48]. Yang et al. showed that inhibiting BNSTpr^{Esr1} cells can perturb male aggression and sexual behaviors, although their function in females was not tested[49]. Zhou et al. found estrogen receptor 2 expressing BNST cells (BNSTpr^{Esr2}), a subpopulation of BNSTpr^{Esr1} cells, mediates sexual satiey in both males and females[48,50]. Thus, probably not all BNSTpr^{Esr1} cells mediate infanticide. The molecular identity of infanticide-relevant BNSTpr cells is likely to be refined in future studies (Supplementary Note 2).

A negative circuit that counteracts the maternal circuit has long been suspected[5,6]. Here, our study unequivocally demonstrated the existence of an infanticide circuit in females and revealed its plasticity over the reproductive state and its variability among individuals with different propensity to kill pups. Our study further uncovered the intimate and antagonistic relationship between infanticide and maternal circuits, highlighting the importance of studying both circuits to understand the generation of infant-directed behaviors under normal and pathological conditions.

Methods

Mice

All procedures were approved by the NYULMC Institutional Animal Care and Use Committee (IACUC) in compliance with the National Institutes of Health (NIH) Guidelines for the Care and Use of Laboratory Animals. Adult male mice (8–16 weeks) were used as test subjects for all studies. Mice were housed under a 12 h light-dark cycle (dark cycle, 10 a.m. to 10 p.m.), with food and water available ad libitum. Room temperature was maintained between 20 – 22 °C and humidity between 30–70%, with a daily average approximately 45%. Esr1-2A-Cre mice were provided initially by D.J. Anderson lab (Caltech) and are currently available from Jackson Laboratory (stock no. 017911). Esr1-2A-Cre mice with SW background were backcrossed with SW wildtype mice for at least five generations. All experimental Esr1-2A-Cre mice are heterozygous. Ai6 mice were purchased from the Jackson Laboratory (stock no. 007906) and were backcrossed to either SW or C57 for at least five generations. Wildtype SW mice were purchased from Taconic. Wildtype C57BL/6 and Balb/c mice were purchased from Charles River, P1-P5 pups used for behavioral experiments were bred in-house. Mice were housed in 12 h light-dark cycle (10 p.m. – 10 a.m. light), with food and water available ad libitum. All mice were group housed until adulthood. After surgery, mice were single housed unless they were paired with a male, and after they became pregnant, they were single housed again until having a litter.

Virus

AAV2-CAG-Flex-GCaMP6f was purchased from the University of Pennsylvania vector core. AAV2-hSyn-FLEX-GFP, AAV2-hSyn-Flex-ArchT-Tdtomato, AAV2-hSyn-Flex-ChrimsonR-tdTomato, and AAV2-EF1a-DIO-ChR2-EYFP were purchased from the University of North Carolina vector core. AAV1-hSyn-Cre, AAV2-hSyn-DIO-mCherry, AAV2-hSyn-DIO-hM3Dq-mCherry and AAV2-hSyn-DIO-hM4Di-mCherry were purchased from Addgene. AAV8-hSyn-DIO-DTR was purchased from Boston Children's Hospital. The titer of AAV1-hSyn-Cre was higher than 2×10^{13} genomic copies per ml. The titer of other viruses ranged from 2×10^{12} to 2×10^{13} genomic copies per ml.

Stereotactic Surgery

Mice (8–20 weeks old) were anesthetized with 1%–2% isoflurane and positioned on a stereotaxic rig (Kopf Instruments Model 1900). Viruses were delivered into brains through a glass capillary using nanoinjector (World Precision Instruments, Nanoliter 2000).

To investigate infanticide-induced c-Fos expression in MPOA-connected cells, 50 nL AAV1-hSyn-Cre (titer $>2 \times 10^{13}$) and 50 nL AAV2-hSyn-DIO-mCherry were mixed and injected into unilateral MPOA (AP: 0 mm, ML: −0.3 mm, DV: −4.95 mm) of SW Ai6 female mice.

To ablate $MPOA^{Esr1}$ cells, 300 nL AAV8-hSyn-DIO-DTR (Control: AAV2-hSyn-DIO-mCherry) was injected into bilateral MPOA (AP: 0 mm, ML: ±0.3 mm, DV: −4.95 mm) of heterozygous virgin Esr1-2A-Cre female in SW background. To chemogenetically inhibit $MPOA^{Esr1}$ cells, 300 nL AAV2-hSyn-DIO-hM4Di-mCherry (Control: AAV2-hSyn-DIO-mCherry) was injected into bilateral MPOA (AP: 0 mm, ML: ±0.3 mm, DV: −4.95 mm) of heterozygous virgin Esr1-2A-Cre female in SW background. All female mice were screened prior to surgery, and only females that did not show spontaneous infanticide were used.

To chemogenetically activate MPOA-connecting cells in various brain regions, we injected 200 nL 1:1 mixture of AAV1-hSyn-Cre (titer $>2 \times 10^{13}$) and AAV2-hSyn-Flex-GFP into bilateral MPOA (AP: 0 mm, ML: ±0.3 mm, DV: −4.95 mm), and at the same time AAV2-hSyn-DIO-hM3Dq-mCherry into bilateral BNSTpr (AP: −0.45 mm, ML: ±0.9 mm, DV: −3.6 mm; 300 nL/side), MeApd (AP: −2.0 mm, ML: ±2.25 mm, DV: −4.6 mm; 200 nL/side), PVT (AP: −0.96 mm, ML: ±0.2 mm, DV: −3.17 mm; 100 nL/side), PVN (AP: −0.6 mm, ML: ±0.3 mm, DV: −4.3 mm; 100 nL/side), VMHvl (AP: −1.8 mm, ML: ±0.75 mm, DV: −5.6 mm; 50 nL/side), PMv (AP: −2.35 mm, ML: ±0.5 mm, DV: −5.6 mm; 200 nL/side) or SUM (AP: −3.06 mm, ML: ±0.4 mm, DV: −4.7 mm; 100 nL/side). For control females, AAV2-hSyn-DIO-mCherry was injected into the target region.

To chemogenetically inhibit $BNSTpr^{Esr1}$ neurons, we injected AAV2-hSyn-DIO-hM4Di-mCherry (control: AAV2-hSyn-DIO-mCherry) bilaterally into the BNSTpr (AP: −0.45 mm, ML: ±0.9 mm, DV: −3.6 mm; 300 nL/side) of adult virgin Esr1-2A-Cre female in SW background.

To optogenetically activate $BNSTpr^{MPOA}$ neurons, we injected 200 nL 1:1 mixture of AAV1-hSyn-Cre (titer $> 2 \times 10^{13}$) and AAV2-hSyn-Flex-GFP bilaterally into MPOA (AP:

0 mm, ML: ±0.3 mm, DV: −4.95 mm), and at the same time AAV2-EF1a-DIO-ChR2-EYFP bilaterally into BNSTpr (AP: −0.45 mm, ML: ±0.9 mm, DV: −3.6 mm; 300 nL/side) of adult C57BL/6 females. To optogenetically activate BNSTpr^{Esr1} neurons, we injected AAV2-EF1a-DIO-ChR2-EYFP bilaterally into BNSTpr (AP: −0.45 mm, ML: ±0.9 mm, DV: −3.6 mm; 300 nL/side) of adult virgin Esr1-2A-Cre females of C57BL/6 and SW background. During the surgery and after virus injection, two 200-μm optical fibers (Thorlabs, FT200EMT, CFLC230) were inserted 500 μm above the virus injection sites, one into each side, and secured on the skull using adhesive dental cement (C&B Metabond, S380). SW adult female mice were screened before surgery to ensure no spontaneous infanticide.

To optogenetically inactivate BNSTpr^{Esr1} projection to MPOA, we injected AAV2-hSyn-Flex-ArchT-Tdtomato (control: AAV2-hSyn-DIO-mCherry) bilaterally into BNSTpr (AP: −0.45 mm, ML: ±0.9 mm, DV: −3.6 mm; 300 nL/side) of Esr1-2A-Cre female with SW background. During the same surgery, two 400-μm optical fibers (Doric, DFC_400/430) were inserted 500 μm above MPOA (AP: 0 mm, ML: ±0.3 mm, DV: −4.45 mm), one on each side, and secured on the skull using adhesive dental cement (C&B Metabond, S380). All female mice were screened before surgery, and only females that showed spontaneous infanticide were used.

To optogenetically inactivate MPOA^{Esr1} projection to BNSTpr, we injected AAV2-hSyn-Flex-ArchT-Tdtomato (Control: AAV2-hSyn-DIO-mCherry) bilaterally into MPOA (AP: 0 mm, ML: ±0.3 mm, DV: −4.95 mm; 300 nL/side) of Esr1-2A-Cre female with SW background. During the surgery and after virus injection, two 200-μm optical fibers (Thorlabs, FT200EMT, CFLC230) were inserted 500 μm above BNSTpr (AP: −0.45 mm, ML: ±0.9 mm, DV: −3.1 mm), one on each side, and secured on the skull using adhesive dental cement (C&B Metabond, S380). All female mice were screened before surgery, and only females that did not show spontaneous infanticide were used.

To optogenetically activate BNSTpr^{Esr1} projection to MPOA, we injected AAV2-hSyn-Flex-ChrimsonR-tdTomato (group 1) or AAV2-EF1a-DIO-ChR2-EYFP mixed with AAV2-hSyn-DIO-hM4Di-mCherry (group 2) bilaterally into BNSTpr (AP: −0.45 mm, ML: ±0.9 mm, DV: −3.6 mm; 300 nL/side for group 1, 500 nL/side for group 2). During the surgery and after virus injection, two 400-μm optical fibers (Doric, DFC_400/430) were inserted 500 μm above MPOA (AP: 0 mm, ML: ±0.3 mm, DV: −4.45 mm), one on each side, and secured on the skull using adhesive dental cement (C&B Metabond, S380). Control females were injected with AAV2-hSyn-DIO-mCherry. Control and group 1 female mice were screened prior to surgery, and only females that did not show spontaneous infanticide were used. Group 2 female mice were screened before surgery, and only females that showed spontaneous pup retrieval were used.

To optogenetically activate MPOA^{Esr1} projection to BNSTpr, we injected AAV2-hSyn-Flex-ChrimsonR-tdTomato (group 1) or AAV2-EF1a-DIO-ChR2-EYFP mixed with AAV2-hSyn-DIO-hM4Di-mCherry (group 2) bilaterally into MPOA (AP: 0 mm, ML: ±0.3 mm, DV: −4.95 mm; 300 nL/side for group 1, 500 nL/side for group 2). During the surgery and after virus injection, two 200-μm optical fibers (Thorlabs, FT200EMT, CFLC230) were inserted

500 μm above BNSTpr (AP: −0.45 mm, ML: ±0.9 mm, DV: −3.1 mm), one on each side, and secured on the skull using adhesive dental cement (C&B Metabond, S380). Control females were injected with AAV2-hSyn-DIO-mCherry. All female mice were screened before surgery, and only infanticidal females were used.

To record Ca^{2+} signal of $MPOA^{Esr1}$ or $BNSTpr^{Esr1}$ cells, 300 nL AAV2-CAG-Flex-GCaMP6f (control: AAV2-hSyn-Flex-GFP) was injected into unilateral MPOA (AP: 0 mm, ML: −0.3 mm, DV: −4.95 mm) or BNSTpr (AP: −0.45 mm, ML: −0.9 mm, DV: −3.6 mm) of heterozygous virgin Esr1-2A-Cre female in SW background. To record Ca^{2+} signals of $BNSTpr^{MPOA}$ cells, 100 nL AAV1-hSyn-Cre (titer $>2\times10^{13}$) and 100 nL AAV2-hSyn-DIO-mCherry were mixed and injected into unilateral MPOA (AP: 0 mm, ML: −0.3 mm, DV: −4.95 mm), at the same time 300 nL AAV2-CAG-Flex-GCaMP6f was injected unilaterally into BNSTpr (AP: −0.45 mm, ML: −0.9 mm, DV: −3.6 mm) of WT virgin SW females. After virus injection, a 400-μm optical fiber assembly (Thorlabs, FR400URT, CF440) was inserted 300 μm above the virus injection site and secured on the skull using adhesive dental cement (C&B Metabond, S380). Recording started at least 3 weeks after surgery.

To simultaneously record Ca^{2+} signal of $MPOA^{Esr1}$ or $BNSTpr^{Esr1}$ cells, 300 nL AAV2-CAG-Flex-GCaMP6f was injected into unilateral MPOA (AP: 0 mm, ML: −0.3 mm, DV: −4.95 mm) and contralateral BNSTpr (AP: −0.45 mm, ML: +0.9 mm, DV: −3.6 mm) of heterozygous virgin Esr1-2A-Cre female in SW background. After the virus injection, an optical fiber assembly that contains two 100-μm optic fibers (USCONEC, C12405, Ferrule_48F) was secured on the skull using adhesive dental cement (C&B Metabond, S380). The optic fibers ended 50 μm above the virus injection sites. Recording started at least 4 weeks after surgery.

For anterograde tracing of $BNSTpr^{Esr1}$ and $MPOA^{Esr1}$ neurons, 50 nL AAV2-hSyn-FLEX-GFP was injected unilaterally into BNSTpr (AP: −0.45 mm, ML: −0.9 mm, DV: −3.6 mm) or MPOA (AP: 0 mm, ML: −0.3 mm, DV: −4.95 mm) of virgin Esr1-2A-Cre females with SW background.

To examine the synaptic connection from $BNSTpr^{Esr1}$ cells to $MPOA^{Esr1}$ cells using slice electrophysiology, we injected AAV2-EF1a-DIO-ChR2-EYFP into bilateral BNSTpr (AP: −0.45 mm, ML: ±0.9 mm, DV: −3.6 mm; 300 nL/side), and at the same time injected AAV2-hSyn-DIO-mCherry bilaterally into MPOA (AP: 0 mm, ML: ±0.3 mm, DV: −4.95 mm; 300 nL/side). To examine $MPOA^{Esr1}$ to $BNSTpr^{Esr1}$ projection, we injected AAV2-EF1a-DIO-ChR2-EYFP bilaterally into MPOA (AP: 0 mm, ML: ±0.3 mm, DV: −4.95 mm; 300 nl/side), and at the same time AAV2-hSyn-DIO-mCherry into bilateral BNSTpr (AP: −0.45 mm, ML: ±0.9 mm, DV: −3.6 mm; 300 nL/side). All mice were heterozygous virgin Esr1-2A-Cre females with SW background.

To examine the intrinsic properties of $MPOA^{Esr1}$ and $BNSTpr^{Esr1}$ cells, we injected AAV2-hSyn-FLEX-GFP bilaterally into MPOA (AP: 0 mm, ML: ±0.3 mm, DV: −4.95 mm; 300 nl/side) and BNSTpr (AP: −0.45 mm, ML: ±0.9 mm, DV: −3.6 mm; 300 nl/side) in each animal. All mice were heterozygous virgin Esr1-2A-Cre females with SW or C57BL/6 background.

To validate ArchT-mediated terminal inactivation for MPOA^{Esr1}—BNSTpr pathway, we injected a mixture of 150 nL AAV2-hSyn-Flex-ArchT-Tdtomato and 150 nL AAV2-EF1a-DIO-ChR2-EYFP into bilateral MPOA (AP: 0 mm, ML: −0.3 mm, DV: −4.95 mm), and at the same time 200 nL AAV2-CAG-Flex-GCaMP6f into bilateral BNSTpr (AP: −0.45 mm, ML: +0.9 mm, DV: −3.6 mm) of SW virgin Esr1-2A-Cre female mice. To validate ArchT-mediated terminal inactivation for BNSTpr^{Esr1}—MPOA projection, we injected a mixture of 150 nL AAV2-hSyn-Flex-ArchT-Tdtomato and 150 nL AAV2-EF1a-DIO-ChR2-EYFP into bilateral BNSTpr (AP: −0.45 mm, ML: +0.9 mm, DV: −3.6 mm), and 200 nL AAV2-CAG-Flex-GCaMP6f into bilateral MPOA (AP: 0 mm, ML: −0.3 mm, DV: −4.95 mm) of SW Esr1-2A-Cre female mice.

MPOA^{Esr1} cell ablation

SW females were prescreened, and only non-infanticide females were used for surgery. During the screening, 2 pups were introduced into the home cage of the test female mouse for 10 min. 3 weeks after surgery, we tested the behaviors towards the pups on the day before diphtheria toxin injection. During the test, 2 P1-P5 pups were introduced into the test female's home cage at a location distant from the nest for 10 minutes. After the test, we injected diphtheria toxin (50 μg/kg, 5μg/kg dissolved in PBS) intraperitoneally into each female. 7 days later, females were tested again by introducing 2 P1-P5 pups into the test female's home cage at a location distant from the nest, wounded pups were euthanized and test was stopped if females attacked them and caused physical damage in the 10 minutes testing period.

Pharmacogenetic activation and inactivation

For pharmacogenetic inhibition of MPOA^{Esr1} cells, SW females were screened before the surgery by introducing 2 pups into the home cage of the female for 10 min. Only females that did not attack pups during the screening were used for surgery. 3 weeks after virus injection, sterile saline or CNO (1 mg/kg) was injected intraperitoneally 30 min prior to behavioral assays on separate days. Saline was always injected the day before CNO injection. During the test, 2 P1-P5 pups were introduced into the test female's home cage at a location distant from the nest for 10 minutes, if the tested females attack and caused physical damage to pups in the 10 minutes testing period, the test was stopped, and wounded pups were immediately euthanized.

For pharmacogenetic activation of MPOA-connecting cells in BNSTpr, MeApd, PVT, PVN, VMHvl, PMv and SUM, females were not screened as infanticide is very rare in C57BL/6 females. 3 weeks after virus injection, sterile saline or CNO (1 mg/kg) was injected intraperitoneally 30 min prior to behavioral assays on separate days. Saline was always injected the day before CNO injection. During the 10 min behavior test, 3 P1-P5 pups were introduced into the test female's home cage for 10 min at a location distant from the nest. We euthanized the pups immediately after the test if they were attacked by the females.

For pharmacogenetic inhibition of BNSTpr^{Esr1} neurons assay, 16 hM4Di and 16 mCherry control females were tested in the virgin state. Among them, 9 hM4Di and 8 mCherry virgin females showed spontaneous infanticide, and they constitute the infanticide group shown

in Figure 2q; 6 hM4Di and 5 mCherry virgin females ignored pups, and they constitute the non-infanticidal animals shown in Extended Data Figure 8b. 3 weeks after surgery, we injected saline and then 1 day later CNO (1 mg/kg). 30 min after injection, we introduced 3–4 pups into the home cage of the female for 10 minutes if there is no attack happens, and if the tested females attack and caused physical damage to pups in the 10 minutes testing period, the test was stopped, and wounded pups were immediately euthanized. After completing the test under a virgin state, each female was paired with a male until they became visibly pregnant. 11 hM4Di and 9 mCherry females became mothers. All 11 hM4Di and 8 mCherry lactating females showed maternal aggression. For the pup interaction test in lactating females (postpartum days 3 and 4), we removed all pups from the cage and injected either saline or CNO on separate days. 30 min after drug injection, 5 pups were introduced into the test female's home cage for 10 min. Afterwards, we removed all pups, and introduced an adult group-housed Balb/c female into the test female's home cage for 10 min followed by an adult Balb/c male for 10 min with 10 min in between.

Optogenetic activation

For $BNSTpr^{MPOA}$ optogenetic activation, 11 and 8 WT C57BL/6 virgin adult female mice were injected with ChR2 and GFP viruses, respectively. For $BNSTpr^{Esr1}$ optogenetic activation, 8 C57BL/6 and 5 SW Esr1-2A-Cre virgin females were injected with ChR2 virus, and 8 C57BL/6 virgin Esr1-2A-Cre females were injected with GFP virus. For ChR2 mice, after testing in the virgin state, each was paired with a male. 6 C57BL/6 females and 4 SW Esr1-2A-Cre females became mothers and were tested again during lactation. Esr1-2A-Cre SW females were screened before the surgery, and only females that did not show infanticide were used.

Three weeks after surgery, the implanted optic fiber assembly was coupled to a patch cord using a zirconia split sleeve (Thorlab, ADAL1-5) to deliver 473 nm laser pulses to the brain. The laser pulses were controlled by TTL signals generated using an RP2 processor (TDT). Regardless of the intruder type, for each test session, 9 sham stimulation (0 mW, 20 s) was first delivered, followed by 9 light stimulation trials at each laser intensity (20 ms, 20 Hz, 20 s, 0.5, 1, 2, 3, 4, and 5 mW). The inter-trial interval was approximately 60 s, although it could be longer sometimes due to replacing wounded pups. For testing pup-directed behaviors in virgins, we introduced 3–4 P1-P5 pups at the beginning of a session. When testing in lactating females, all pups of the dam were removed 10 min before the test session and reintroduced right before the session started. If a pup was attacked, we replaced it with a new one and euthanized the wounded pup. For adult female and male sessions, an adult group housed Balb/c female, then a Balb/c male was introduced, and sham and light stimulation were delivered using the same stimulation protocol during the pup interaction test. The first pulse train started for both sham and stimulation trials at a given laser intensity when the testing female investigated the intruder.

For the RTPP test, sham then 20 ms, 20 Hz, 3 mW light pulses were delivered whenever the animal entered the pre-designated stimulation chamber and terminated when the animal moved out of the chamber. Each test lasted for 10 min. For the EPM test, mice were habituated to the test area for two days, 20 min a day. During the test, we delivered no

light for the first 20 minutes, then 3 mW light pulses for 20 min. The body center of the animal was tracked with DeepLabCut[51] and used for calculating the time animal spent in each chamber in the RTPP test and the open/closed arms in the EPM test.

Optogenetic terminal activation and inhibition

For BNSTpr^{Esr1}–MPOA terminal inhibition, we prescreened SW Esr1-2A-Cre virgin females before the surgery and only used females that showed spontaneous infanticide for surgery. For MPOA^{Esr1}–BNSTpr terminal inhibition, we only used SW Esr1-2A-Cre virgin females that did not show spontaneous infanticide for surgery. 4 weeks after virus injection, we introduced 2 P1-P5 pups into the female's home cage, far from the nest, for 10 minutes if there is no attack happens, and if the tested females attack and caused physical damage to pups in the 10 minutes testing period, the test was stopped, and wounded pups were immediately euthanized. During the pup interaction test, we continuously delivered either sham (0 mW) or 5 mW 589 nm light (Shanghai Dream Laser). The sham stimulation session occurred on the day before the light stimulation session. If the female attacked a pup, we euthanized the pup after the test.

For BNSTpr^{Esr1}–MPOA terminal activation (without BNSTpr^{Esr1} inhibition), we only used females that did not show spontaneous infanticide during the pre-surgery pup interaction test. For MPOA^{Esr1}–BNSTpr activation (without MPOA^{Esr1} inhibition), we only used females that showed spontaneous infanticide before surgery. 4 weeks after the surgery, we introduced 2 pups into the female's home cage for 10 minutes if there is no attack happens, and if the tested females attack and caused physical damage to pups in the 10 minutes testing period, the test was stopped, and wounded pups were immediately euthanized. We delivered either sham (0 mW) or 5 mW 20 ms 20 Hz 589 nm light pulses during the entire session. The sham stimulation session occurred on the day before the light situation session.

For BNSTpr^{Esr1}—MPOA terminal activation and simultaneous BNSTpr^{Esr1} inhibition, we only used females that showed spontaneous retrieval before surgery. For MPOA^{Esr1}—BNSTpr terminal activation and simultaneous MPOA^{Esr1} inhibition, we only used spontaneous infanticidal females. 4 weeks after surgery and on the day of testing, we i.p. injected CNO (1 mg/kg) and 30 min later, introduced 2 pups (P1-P5) into the female's home cage and delivered sham (0 mW) or 20 ms 20 Hz 473 nm light for 10 min. If a pup was attacked by the female, it would be euthanized after the test.

After the pup interaction test, for BNSTpr^{Esr1}-MPOA (both with and without BNSTpr^{Esr1} inhibition) animals, an adult group-housed Balb/c female and then a Balb/c male was introduced, and the same light stimulation protocol was applied.

After completing the behavior experiments and on a separate day, we delivered 5 mW 20 ms 20 Hz 589 nm light pulses for 10 min to one side of the MPOA or BNSTpr of ChrimsonR animals. We i.p. injected CNO (1 mg/kg) to ChR2+Gi animals and then 30 min later delivered 5 mW 20 ms 20 Hz 473 nm light pulses to one side of the MPOA or BNSTpr for 10 min. 90 min after the light delivery, we perfused the animal and collected the brain for c-Fos staining.

Behavioral analyses

Animal behaviors were recorded from both top and side using two synchronized cameras (Edmund, stock #89533) controlled by StreamPix (NORPIX) at 25 frames/sec. Behaviors were manually annotated frame-by-frame using custom software written in MATLAB (https://pdollar.github.io/toolbox/). “Approach pup” is when the testing female faces and walks straight to the pup. “Investigate pup” is when the female’s nose closely contacts any body parts of a pup. “Attack pup” is defined as biting a pup and is confirmed by the wounds. “Retrieve pup” is defined as the moment the female lifts the pup using its jaw to the moment the pup is dropped in or around the nest. “Groom pup” is defined as close interaction between the female and pup accompanied by rhythmic up and down head movement of the female and displacement of the pup. “Investigate female/male” is defined as nose-to-face, nose-to-trunk, or nose-to-urogenital contact. “Social groom” is defined as licking or grooming the head or neck area of the adult intruder. “Mount” is when the testing female mouse clasps onto the flank of the adult intruder, establishes an on-top position, and moves its pelvis rhythmically. “Attack female/male” is defined as lunging, biting, and fast movements connecting these behaviors.

Estrous state determination

We washed the vaginal area of the female mouse using 50 uL saline several times, mounted the washed solution on a slide, and examined the cell morphology under a light microscope to determine the females’ estrous state. If the vaginal cytology showed the presence of mainly cornified epithelial cells, the female mouse was determined to be in estrus; If leukocytes were the main cell type in vaginal cytology, the female mouse was determined to be in diestrus.

Fiber photometry

For single region fiber photometry recording, the fluorescence signals were as described previously[43,45]. Briefly, 390-Hz sinusoidal blue LED light (30 μW; LED light: M470F1; LED driver: LEDD1B; from Thorlabs) was bandpass filtered (passing band: 472 ± 15 nm, FF02-472/30-25, Semrock) and delivered to the brain to excite GCaMP6f. The emission light traveled back through the same optic fiber, bandpass filtered (passing bands: 535 ± 25 nm, FF01-535/505, Semrock), passed through an adjustable zooming lens (Thorlab, SM1NR01 and Edmund optics, #62-561), detected by a Femtowatt Silicon Photoreceiver (Newport, 2151), and recorded using a real-time processor (RP2, TDT). The envelope of the 390-Hz signals reflected the intensity of the GCaMP and was extracted in real-time using a custom TDT program. The signal was low pass filtered with a cut-off frequency of 10 Hz. The blue LED was adjusted so that the light intensity at the tip of the optical fiber was 30 μW. The baseline fluorescence was set around 1 (arbitrary unit) for all animals by adjusting the zooming lens attached to the photoreceiver.

For fiber photometry recording of $MPOA^{Esr1}$ neurons, 11 females were injected with AAV2-CAG-Flex-GCaMP6f. 5 out of 11 females showed infanticide 3 weeks after surgery, and were used for recording. For virgin females, all recordings were done during diestrus, which was determined based on vaginal cytology. During the first recording session, animals were left alone in their home cage for around 10 minutes, and then a P1-P5 pup was introduced at

a location distant from the nest. After naturally occurring infanticide, the pup was removed and euthanized. A total of 3–5 pups were introduced during the recording session, each for approximately 1–2 minutes. After the recording session with pups, we introduced a group-housed adult Balb/c female mouse and then an adult Balb/c male mouse into the cage of the recording female mouse, each for 10 minutes with 10 minutes in between. After recording in a hostile virgin state, females were exposed to pups for more than 30 min each day for 1–2 weeks. During the first 3–7 days of pup sensitization, pups were presented under a cup to prevent infanticide. Once females stopped infanticide, they were allowed to freely interact with 3–5 pups for another 2–7 days until they quickly retrieved all pups back to nest on two consecutive days. Then we performed fiber photometry recordings again. During the recording, 3–5 pups were introduced into the female's cage far from the nest for approximately 10 minutes. Then, adult male and female intruders were introduced sequentially in the same way as the recording under the hostile virgin state. After completing both recording sessions, we paired each female with an adult male until the female became visibly pregnant. On postpartum day 2 or 3, mothers were recorded with the same procedure as in the maternal virgin state.

For fiber photometry recording of $BNSTpr^{Esr1}$ neurons, 14 females that were injected with AAV2-CAG-Flex-GCaMP6f showed the proper virus expression and fiber placement. 8 out of 14 females showed infanticide, and 7 out of 8 females became mothers. So, 7 females were recorded from virgin to lactating state. For fiber photometry recording of $BNSTpr^{MPOA}$ neurons, 6 females were recorded from virgin to lactating state. The recording procedure was the same for recording $MOPA^{Esr1}$ cells in hostile virgin females and mothers. Control GFP animals underwent the same recording protocol.

For simultaneous recording of $MPOA^{Esr1}$ and $BNSTpr^{Esr1}$ neurons, we injected viruses into 6 females. 3 out of 6 females had correct virus expression and fiber placements in both regions, showed infanticide in the virgin state, and became mothers. The muti-fiber recording setup was the same as described in our previous study[52]. Briefly, blue LED light (Thorlabs, M470F1, LEDD1B) was bandpass filtered (Semrock, FF02-472/30-25), reflected on a dichroic filter (Semrock, FF495-Di03-25×36), and coupled into a custom designed 100-μm fiber bundle (Doric Lenses) through an Olympus PLN 10x objective (Edmunds, Stock #86-813). Emission light was bandpass filtered (Semrock, FF01-535/50) and projected onto the CCD sensor of a camera (Basler, acA640-120gc) via an achromatic doublet (Thorlabs, AC254-060-A-ML). The LED was driven by DC current, and the light intensity at the tip of the fiber was set to be ~30 μW. The sampling rate of the camera was 25 frames/s. After video acquisition, we calculated the average pixel value at each fiber end as the raw fluorescence signal (F_{raw}).

During the recording in the virgin state, after recording the baseline activity for 10 min, one pup was introduced into the recording female home cage, and after naturally occurring infanticide, we removed and euthanized the pup and introduced a new pup into the cage. Up to 5 pups were introduced during each recording session, which lasted approximately 15 min. During the recording in the lactating state, all pups were taken out and then introduced into the cage one by one over 15 min.

To analyze the recording data, the MATLAB function “msbackadj” with a moving window of 25% of the total recording duration was first applied to the raw Ca^{2+} signal F_{raw} to get the flatted signal F_{flat}. Then the instantaneous baseline signal was obtained as “$F_{baseline} = F_{raw} – F_{flat}$”. The ΔF/F was then calculated as “$\Delta F/F = (F_{raw} – F_{baseline})/F_{baseline}$”. The Z-scored ΔF/F was then calculated as “$Z = (x-\mu)/\sigma$” (μ: mean of ΔF/F, σ: standard deviation of ΔF/F). The PETHs were constructed by aligning the Z-scored ΔF/F to the onset of each trial of a behavior, averaging across all trials for each animal and then averaging across animals. For each recording session, the responses during a behavior period were calculated as the area under curve (AUC) per second during all trials of a behavior.

In vitro electrophysiological recording

For *in vitro* whole-cell patch-clamp recordings, mice were anesthetized with isoflurane, and brains were removed and submerged in ice-cold cutting solution containing (in mM): 110 choline chloride, 25 $NaHCO_3$, 2.5 KCl, 7 $MgCl_2$, 0.5 $CaCl_2$, 1.25 NaH_2PO_4, 25 glucose, 11.6 ascorbic acid and 3.1 pyruvic acid. 275-μm coronal sections were cut on a Leica VT1200s vibratome and incubated in artificial cerebral spinal fluid (ACSF) containing (in mM): 125 NaCl, 2.5 KCl, 1.25 NaH_2PO_4, 25 $NaHCO_3$, 1 $MgCl_2$, 2 $CaCl_2$ and 11 glucoses at 34°C for 30 min and then at room temperature until use. The intracellular solution for current-clamp recording contained (in mM): 145 K-gluconate, 2 $MgCl_2$, 2 Na_2ATP, 10 HEPES, 0.2 EGTA (286 mOsm, pH 7.2). The intracellular solution for the voltage clamp recording contained (in mM): 135 $CsMeSO_3$, 10 HEPES, 1 EGTA, 3.3 QX-314 (chloride salt), 4 Mg-ATP, 0.3 Na-GTP and 8 sodium phosphocreatine (pH 7.3 adjusted with CsOH). The signals were acquired using MultiClamp 700B amplifier and digitized at 20 kHz with DigiData1550B (Molecular Devices, USA). The recorded electrophysiological data were analyzed using Clampfit (Molecular Devices) and MATLAB (Mathworks).

To determine the intrinsic excitability of $MPOA^{Esr1}$ and $BNSTpr^{Esr1}$ cells, we performed current-clamp recordings and injected 30 current steps ranging from −20 pA to 270 pA in 10 pA increments into the recorded cell. The total number of spikes during each 500-ms long current step was then used to construct F-I curve.

We performed voltage-clamp recordings of $BNSTpr^{Esr1}$ and $MPOA^{Esr1}$ neurons. To record oEPSCs and oIPSCs, the cell membrane potential was held at −70 mV and 0 mV, respectively. To activate ChR2-expressing axons, we delivered brief pulses of full-field illumination (0.5 ms, 0.1Hz, 10 times) onto the recorded cell with a blue LED light (pE-300 white; CoolLED). We then applied TTX (1 μM), 4-AP (100 mM), Gabazine (2 μM), and strychnine (5 μM) through the bath solution sequentially, each for 10–20 minutes. Data acquisition started at least 5 minutes after each drug application.

To validate the ArchT mediated terminal inactivation, we performed voltage-clamp recordings of $BNSTpr^{Esr1}$ (for $MPOA^{Esr1}$–BNSTpr projection) and $MPOA^{Esr1}$ (for $BNSTpr^{Esr1}$–MPOA projection) cells with a holding potential of 0 mV. We activated ChR2-expressing axons by delivering brief blue light pulses (0.5 ms duration, 20 repeats) of full field LED illumination (pE-300 white; CoolLED) and simultaneously delivered 5 mW yellow light (Shanghai dream laser) or not to the recorded cell through a 400 μm optic fiber placed right above the recording site.

Immunohistochemistry and imaging analysis

Mice were perfused with 1 × PBS followed with 4% PFA. Brains were dissected, post-fixed in 4% PFA overnight at 4°C, rinsed with 1 × PBS, and dehydrated in 30% sucrose for 12–16 hours. 30 μm sections were cut on a Leica CM1950 cryostat. For brain-wide c-Fos staining, every one in three brain slices of the whole brain were collected. For Esr1 staining, every one in three brain slices of BNSTpr region were collected. Then, free-floating brain slices were rinsed with PBS (3 × 10 min) and PBST (0.1% Triton X-100 in PBS, 1 × 30 minutes) at room temperature, followed by 1 hour of blocking in 10% normal donkey serum at room temperature. The primary antibody (Guinea pig anti-Fos, 1:500 dilution, Synaptic Systems, Cat. # 226005; Rabbit anti-Esr1, 1:3000 dilution, Millipore, Cat. # 06-935, Lot # 3243424) was diluted in PBST with 3% normal donkey serum and incubated overnight (12–16 hours) at 4°C. Brain slices were then washed with PBST (3 × 10 min) and incubated with the secondary antibody (Secondary antibody for c-Fos staining, Cy3-Goat anti-Guinea pig, 1:500 dilution, Jackson ImmunoResearch, Cat. # 706-165-148; Secondary antibody for Esr1 staining, Cy5-Donkey anti-rabbit, 1:500 dilution, Jackson ImmunoResearch, Cat. # 711-175-152) for 2 hours at room temperature. Then, brain slices were washed with PBST (3 × 10 min), rinsed with 1 × PBS and mounted on superfrost slides (Fisher Scientific, 12-550-15), dried 10 min at room temperature, and coverslipped in 50% glycerol containing DAPI (Invitrogen, Cat. #00-4959-52). Images were acquired using a slide scanner (Olympus, VS120) or a confocal microscope (Zeiss LSM 700 microscope). Brain regions were identified based on Allen Mouse Brain Atlas, and cells were counted manually using ImageJ.

We counted Fos expressing cells in each brain region (note: every third of brain sections were collected for staining) and divided it by the region's size as the density of Fos+ cells. To compare Fos+Tracer+ and Fos-Trace+ cells among different behavior groups, we counted the total Fos+Tracer+ and Fos-Tracer+ cells in each region across all animals and compared the cell numbers across groups. For the relative projection density of $BNSTpr^{Esr1}$ and $MPOA^{Esr1}$ cells, the average fluorescence intensity in each region containing presynaptic GFP+ puncta was first quantified as the average pixel value of the region and then normalized by the average fluorescence intensity of the start region.

Statistics

No statistical methods were used to pre-determine sample sizes but our sample sizes are similar to those reported in previous publications[45,53–56]. All experiments were conducted using 2 to 4 cohorts of animals. The results were reproducible across cohorts and combined for final analysis. All statistical analyses were performed using MATLAB and Prism software. Fisher's exact test was used on unpaired nominal data from two groups. McNemar's test was used on paired nominal data from two groups. All statistical analyses were two-tailed. If distributions passed Kolmogorov–Smirnov or Shapiro-Wilk tests for normality, parametric tests, including paired t-test and one-way ANOVA followed with multiple comparisons test corrected by two-stage linear step-up procedure of Benjamini, Krieger and Yekutieli, were used to determine whether there is any statistically significant difference between the means of two or more groups. For comparing among multiple groups and multiple treatment conditions, two-way repeated measure ANOVA followed

with multiple comparisons tests corrected by two-stage linear step-up procedure of Benjamini, Krieger and Yekutieli were used. If distributions failed to pass normality tests, Mann Whitney test, Wilcoxon matched-pairs signed rank test and mixed-effects analysis followed with multiple comparisons test corrected by two-stage linear step-up procedure of Benjamini, Krieger and Yekutieli were used. For all statistical tests, significance was measured against an alpha value of 0.05. For detailed statistical results, see the statistic summary in each Source Data File.

Extended Data

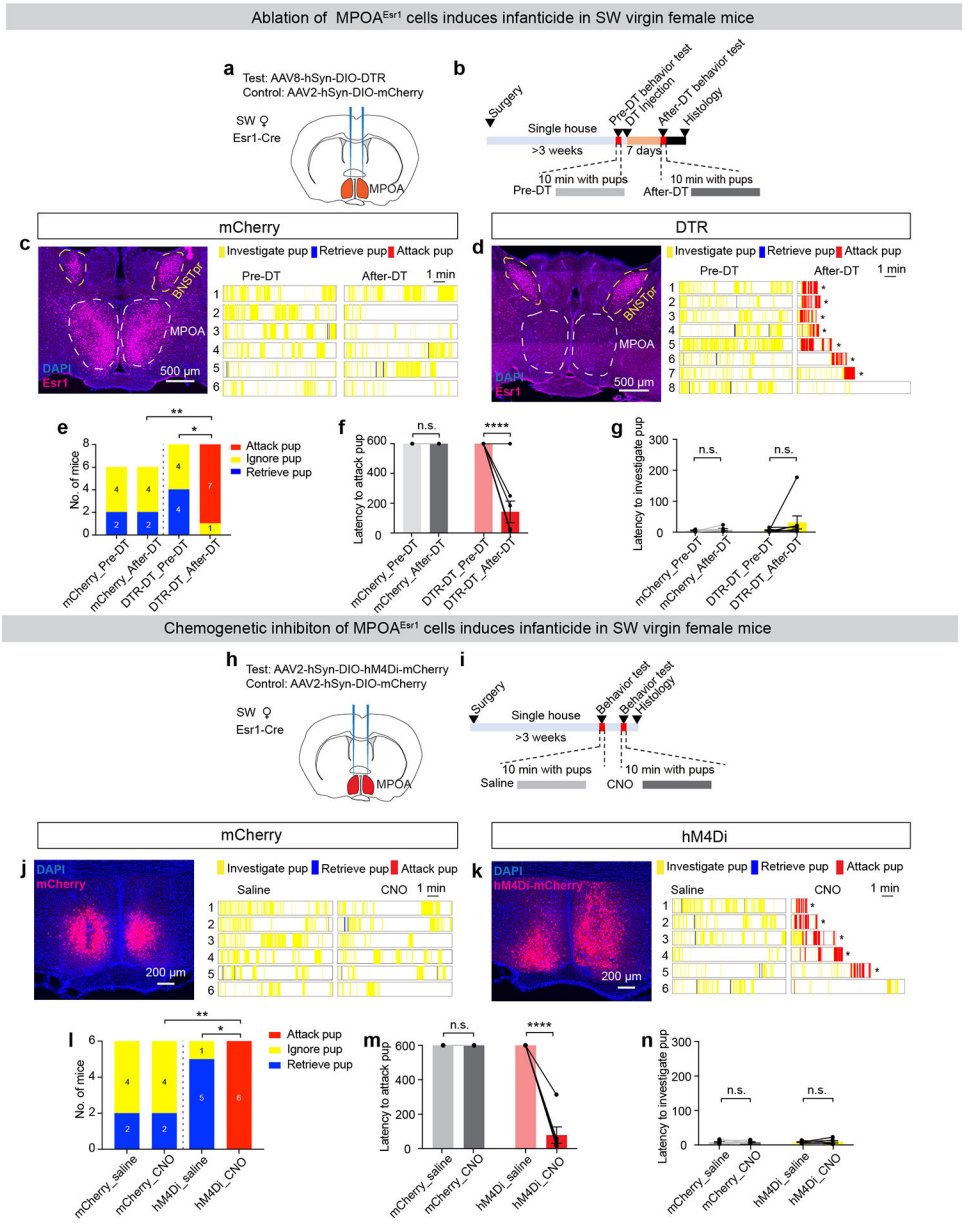

Extended Data Fig. 1: Ablation or chemogenetic inhibition of MPOA^{Esr1} cells induces infanticide in SW virgin female mice

(a) Experimental design to ablate MPOA^{Esr1} cells.
(b) Experimental timeline.
(c, d) Left showing representative histology images of Esr1 staining (magenta) in MPOA and BNSTpr after DT injection in a mCherry female of 6 mice(**c**) and a DTR female of 8 mice (**d**). Right showing raster plots of pup-directed behaviors in mCherry (**c**) and DTR females (**d**) before and after i.p. injection of DT. *Remove wounded pups and stop recording.
(e) Number of mCherry and DTR virgin females that attack, ignore or retrieve pups before and after DT injection. Fisher's exact test for comparing behaviors (attack vs. no attack) between groups before or after DT injection. McNemar's test for comparing behaviors (attack vs. no attack) between pre-DT and after-DT within a group. * $p < 0.05$. **$p < 0.01$.
(f, g) Latency to attack pup (**f**) and investigate pup (**g**) before and after DT injection in mCherry and DTR females. If the behavior of interest is not observed during the entire session, the latency is 600 s. Error bars: ± SEM. Mixed-effects analysis followed with multiple comparisons test. ****$p < 0.0001$. n = 6 mice for mCherry group, n=8 mice for DTR group.
(h) Experimental design to chemogenetically inhibit MPOA^{Esr1} cells.
(i) Experimental timeline.
(j, k) Left showing representative histology images of mCherry (**j**) and hM4Di-mCherry (**k**) expression of 6 mice each group in MPOA. Right showing raster plots of pup-directed behaviors in mCherry (**j**) and hM4Di females (**k**) after i.p. injection of saline or CNO. *Remove wounded pups and stop recording.
(l) Number of mCherry and hM4Di virgin females that attack, ignore or retrieve pups after saline or CNO injection. Fisher's exact test for comparing behaviors (attack vs. no attack) between groups after saline or CNO injection. McNemar's test for comparing behaviors (attack vs. no attack) between saline and CNO injections within a group. * $p < 0.05$. **$p < 0.01$.
(m, n) Latency to attack pup (**m**) and investigate pup (**n**) after saline or CNO injection in mCherry and hM4Di females. Error bars: ± SEM. Mixed-effects analysis (**m**) and Two-way RM ANOVA (**n**) followed with multiple comparisons test. ****$p < 0.0001$. n = 6 mice for each group.
Brain illustrations in (**a**) and (**h**) are produced based on reference atlas from https://atlas.brain-map.org/. See Source Data Extended Data Fig. 1 for detailed values and statistics.

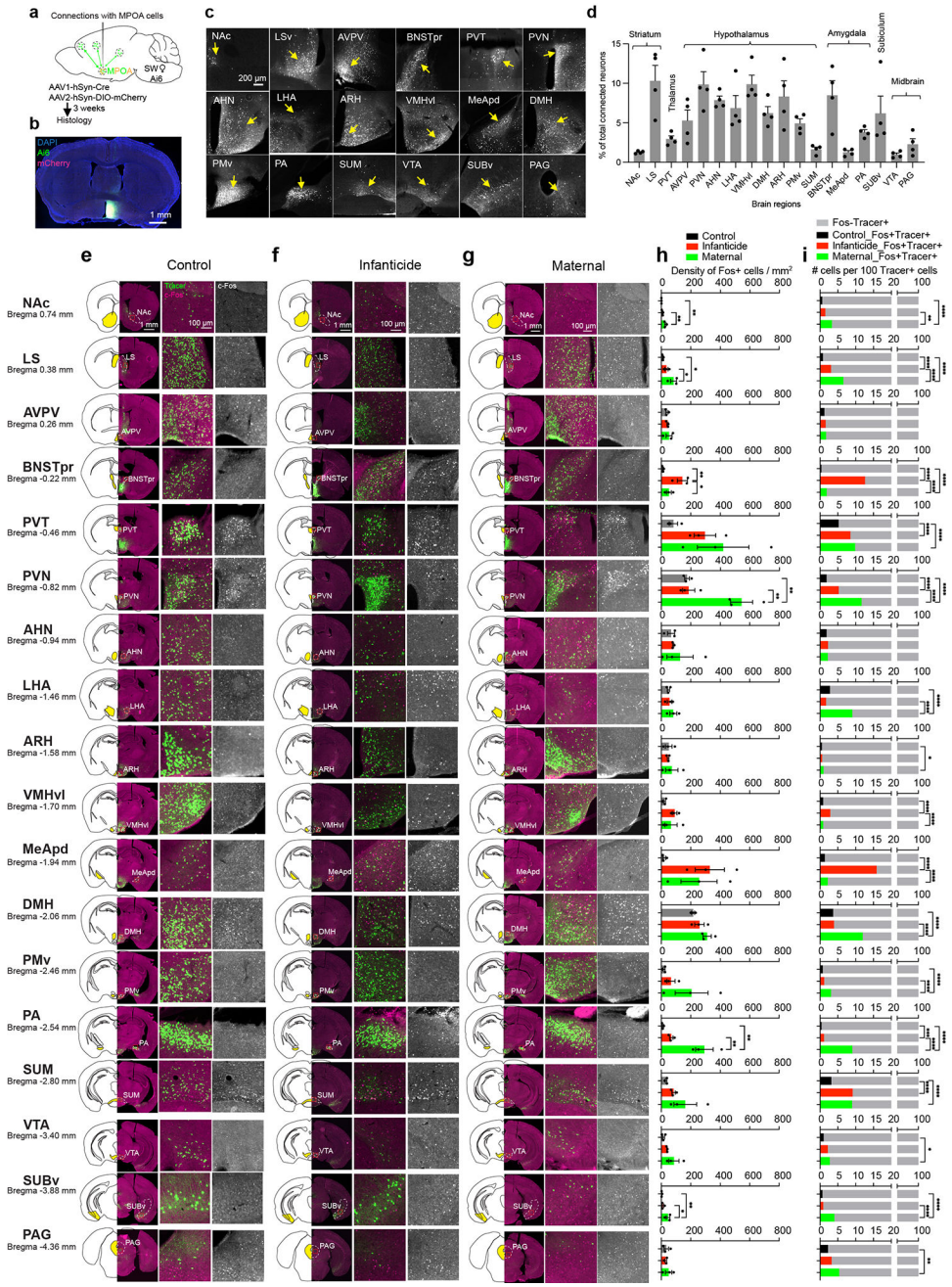

Extended Data Fig. 2: MPOA-connecting cells across brain regions and their overlap with Infanticide and maternal care induced c-Fos.

(a) Experimental design to trace MPOA-connecting cells throughout the brain using Ai6 female mice and high titer (> 1×10^{13} vg/mL) AAV1-hSyn-Cre.

(b and c) Images from a representative animal of 4 mice showing the primary injection site in the MPOA (**b**) and MPOA-connecting cells in various brain areas (**c**). Scale bars: 1 mm (**b**) and 200 μm (**c**).

(d) Distribution of MPOA-connecting neurons in various brain regions. All regions containing over 1% of total labeled cells are shown. n = 4. Error bars: SEM.

(e-g) Representative images of 3 mice each group of 18 regions showing baseline **(e)**, infanticide-induced **(f),** and maternal behavior-induced **(g)** c-Fos and zsGreen expression in Ai6 female mice injected with AAV1-hSyn-Cre into the MPOA. Baseline c-Fos are from females left undisturbed in the home cage. Brain illustrationsare produced based on reference atlas from https://atlas.brain-map.org/.

(h) The density of c-Fos expressing cells in each MPOA-connecting brain region in control, infanticidal and maternal female mice. n = 3 mice for each group. One-way ANOVA followed with multiple comparisons test. *p < 0.05, **p < 0.01, Error bars: ±SEM.

(i) The total number of Fos+Tracer+ and Fos-Trace+ cells per 100 Tracer+ cells in each MPOA-connecting brain region in control, infanticidal and maternal female mice. n = 3 mice for each group. Fisher's exact test is based on unnormalized total numbers of Fos+Tracer+ and Fos-Trace+ cells of each group. *p < 0.05, **p < 0.01, ***p < 0.001, ****p < 0.0001. See Source Data Extended Data Fig. 2 for detailed values and statistics.

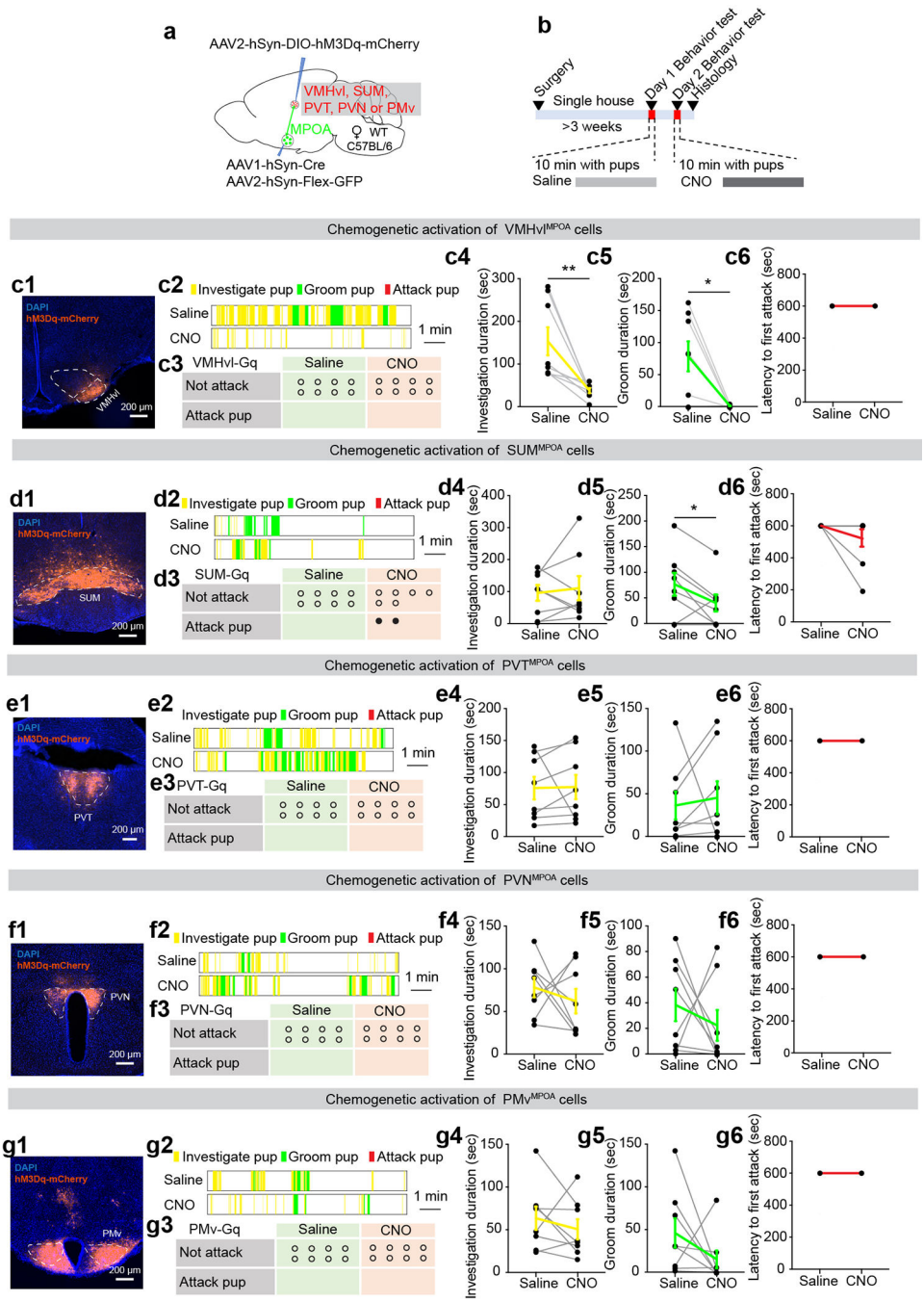

Extended Data Fig. 3: Pup-directed behaviors after chemogenetic activation of MPOA-connecting cells in the VMHvl, SUM, PVT, PVN, or PMv in female mice

(a) Experimental design to chemogenetically activate various MPOA-connecting regions.

(b) Experimental timeline.

(c1, d1, e1, f1, g1) Representative histology images of 8 mice showing hM3Dq-mCherry expression in the VMHvl (**c1**), SUM (**d1**), PVT (**e1**), PVN (**f1**), and PMv (**g1**) after injecting AAV1-Syn-Cre in MPOA and AAV2-hSyn-DIO-hM3Dq-mCherry into each of the regions. Scale bars: 200 μm.

(c2, d2, e2, f2, g2) Representative raster plots showing pup-directed behaviors after saline or CNO injection into animals expressing hM3Dq-mCherry in MPOA-connecting cells in the VMHvl (**c2**), SUM (**d2**), PVT (**e2**), PVN (**f2**), and PMv (**g2**). Each raster lasts 10 min.
(c3, d3, e3, f3, g3) Pup-directed attack after saline or CNO injection in female mice that express hM3Dq-mCherry in MPOA-connecting cells in the VMHvl (**c3**), SUM (**d3**), PVT (**e3**), PVN (**f3**), and PMv (**g3**). Each circle represents one mouse. n = 8 for each group.
(c4, d4, e4, f4, g4) Duration of pup investigation between saline- and CNO-injected days in female mice that express hM3Dq-mCherry in MPOA-connecting cells in the VMHvl (**c4**), SUM (**d4**), PVT (**e4**), PVN (**f4**), and PMv (**g4**). Each gray line represents one animal. The colored line represents the group average. Error bars: ± SEM. Wilcoxon matched-pairs signed rank test (**c4**) or Two-tailed Paired t test (**d4, e4, f4, g4**). **p<0.01. n = 8 for each group.
(c5, d5, e5, f5, g5) Duration of pup grooming between saline- and CNO-injected days in female mice that express hM3Dq-mCherry in MPOA-connecting cells in the VMHvl (**c5**), SUM (**d5**), PVT (**e5**), PVN (**f5**), and PMv (**g5**). Figure conventions as in **c4-g4**.
(c6, d6, e6, f6, g6) Latency to first pup attack between saline- and CNO-injected days in female mice that express hM3Dq-mCherry in MPOA-connecting cells in the VMHvl (**c6**), SUM (**d6**), PVT (**e6**), PVN (**f6**), and PMv (**g6**). Figure conventions as in **c4-g4**.
See Source Data Extended Data Fig. 3 for detailed values and statistics.

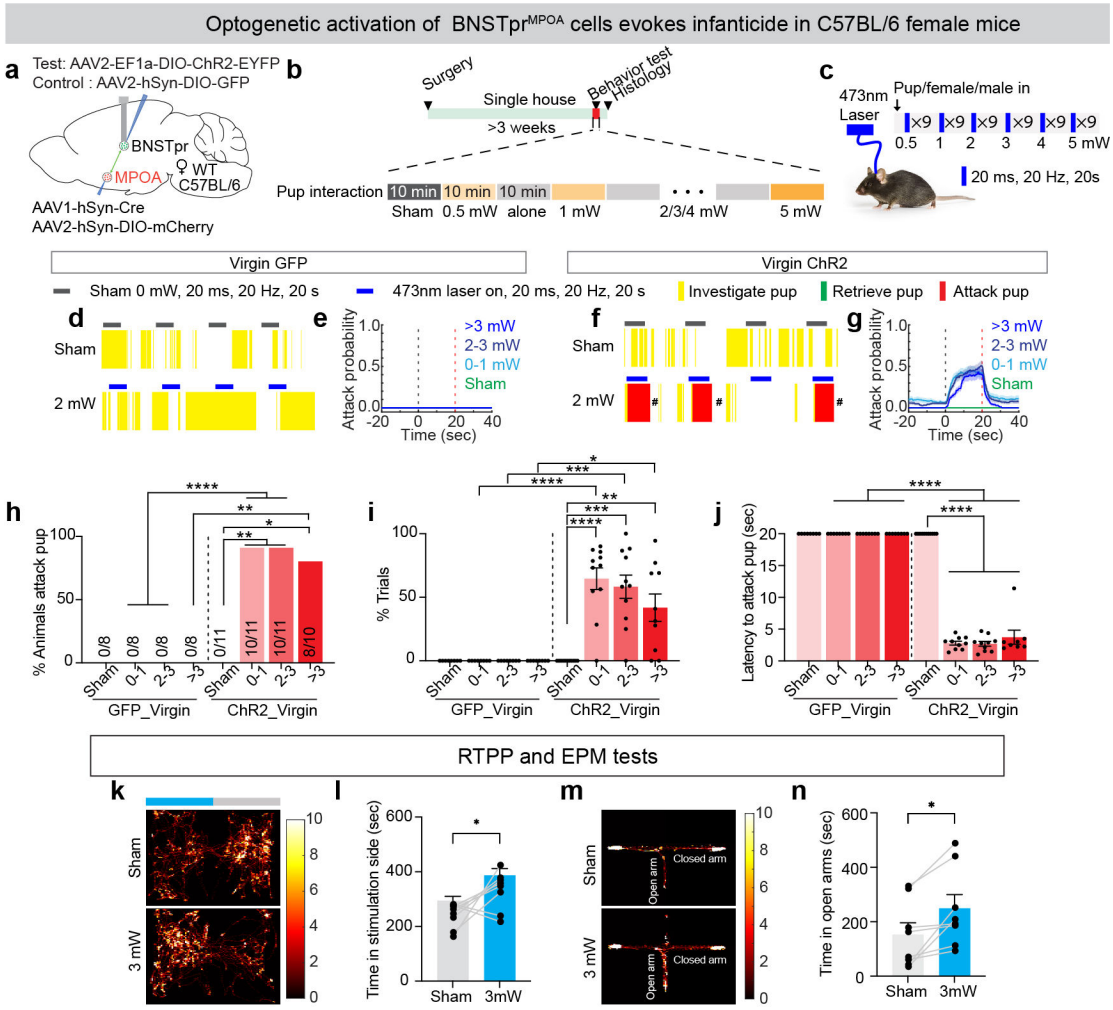

Extended Data Fig. 4: Optogenetic activation of BNSTpr^{MPOA} neurons elicits infanticide, induces real-time place preference, and reduces anxiety in female mice

(a) Experimental design to optogenetically activate BNSTpr^{MPOA} cells.

(b) Experimental timeline.

(c) Light delivery protocol.

(d and f) Representative raster plots showing pup-directed behaviors during sham and 2 mW light stimulation in virgin female mice expressing GFP (**d**) or ChR2-EYFP (**f**) in BNSTpr^{MPOA} cells. # Remove wounded pup(s) and introduce a new pup.

(e and g) PETH of attack pup probability in virgin female mice expressing GFP (**e**) and virgin female mice expressing ChR2-EYFP (**g**) in BNSTpr^{MPOA} cells following sham or light stimulation. Only trials with female-pup contact are included for analysis. Left black dash line: Light on. Right red dash line: light off.

(h) Percentage of animals that attacked pups in GFP and ChR2 group. Fisher's exact test for comparison between GFP and ChR2 group. McNemar's test for comparison between sham and different laser intensity within ChR2 group. *p < 0.05, **p < 0.01, ****p < 0.0001. n = 8 mice for GFP control, n = 11 mice for ChR2 virgin group (sham, 0–1, 2–3), n = 10 mice for ChR2 virgin group (>3).

(i) Percentage of trials showing pup attack. Each dot represents one mouse. Error bars: ± SEM. Mixed-effects analysis followed with multiple comparisons test. *p < 0.05, **p < 0.01, ***p < 0.001, ****p < 0.0001. n = 8 mice for GFP control, n = 11 mice for ChR2 virgin group (sham, 0–1, 2–3), n = 10 mice for ChR2 virgin group (>3).
(j) Averaged latency to attack pup upon encountering the pup following sham or light stimulation. Error bars: ± SEM. Mixed-effects analysis followed with multiple comparisons test. ****p < 0.0001. n = 8 mice for GFP control, n = 11 mice for ChR2 virgin group (sham, 0–1, 2–3), n = 10 mice for ChR2 virgin group (>3).
(k-l) Representative tracking results during the RTPP test (**k**) and the time spent in sham or 3 mW stimulation chamber (**l**). n = 8 mice. Paired t test. *p < 0.05. Error bars: SEM.
(m-n) Representative tracking results during an EPM test (**m**) and the time spent in open arms (**n**) with sham or 3 mW laser stimulation. n = 8 mice. Paired t test. *p < 0.05. Error bars: SEM.
See Source Data Extended Data Fig. 4 for detailed values and statistics.

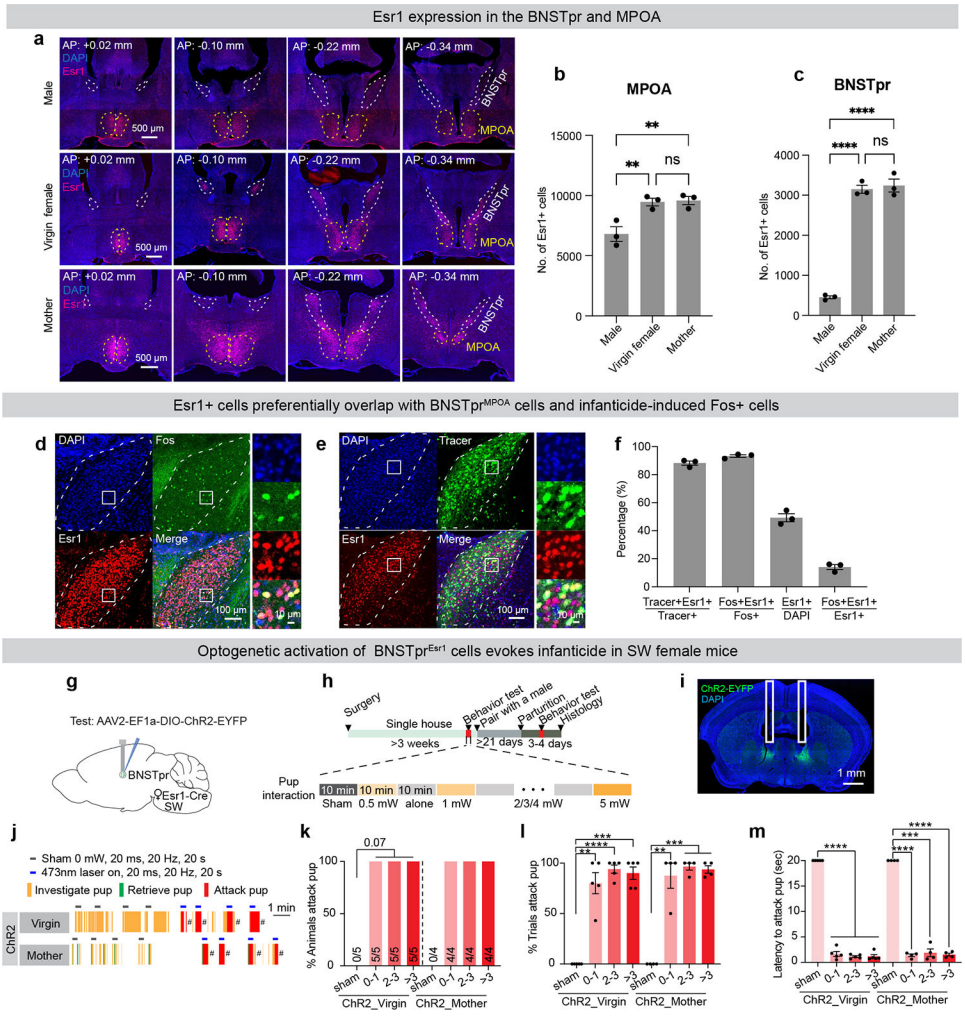

Extended Data Fig. 5: Additional characterization of BNSTpr Esr1 cells and their activation-induced infanticide in SW female mice.

(a) Representative coronal sections of 3 mice each group showing Esr1 immunostaining in MPOA and BNSTpr in a male (top), a virgin female (middle) and a mother (bottom). Scale bars: 500 μm.

(b, c) Number of Esr1 positive cells in the MPOA (**b**) and BNSTpr (**c**) in male, virgin female, and mother mice. n = 3 mice for each group. One-way ANOVA followed with multiple comparisons test. **p < 0.01, ****p < 0.0001. Error bars: ± SEM.

(d) Representative images of 3 mice showing overlap between Esr1 (red) and infanticide-induced c-Fos (green) in the BNSTpr. Right shows the enlarged view of the boxed area. Scale bars: 100 μm (left) and 10 μm (right).

(e) Representative images of 3 mice showing the overlap between Esr1 (red) and zsGreen (green) in the BNSTpr in an Ai6 animals injected with AAV1-hSyn-Cre at the MPOA. Right shows the enlarged view of the boxed area. Scale bars: 100 μm (left) and 10 μm (right).

(f) Quantification of overlap between MPOA-connected cells, Esr1 and the infanticide-induced c-Fos in the BNSTpr. n = 3 mice for each group, Error bars: ± SEM.

(g) Experimental design to optogenetically activate $BNSTpr^{Esr1}$ cells in non-infanticidal SW virgin females.

(h) Experimental timeline.

(i) Representative image of 4 mice showing ChR2 expression (green) in the BNSTpr and fiber tracks (while boxes). Scale bar: 1 mm.

(j) Representative raster plots showing pup-directed behaviors during sham and 2 mW light stimulation in a non-infanticidal SW virgin female (top) and a mother (bottom) expressing ChR2-EYFP in $BNSTpr^{Esr1}$ cells. # Replace a wounded pup.

(k) Percentage of animals that attack pups. n = 5 mice for ChR2 virgin group, n = 4 mice for ChR2 mother group. McNemar's test for comparison between sham and different laser intensity within each ChR2 group.

(l) Percentage of trials showing pup attack. Each dot represents one mouse. Mean ± SEM. Mixed-effects analysis followed with multiple comparisons test. **p < 0.01, ***p < 0.001, ****p < 0.0001. n = 5 mice for ChR2 virgin group, n = 4 mice for ChR2 mother group.

(m) Average latency to attack pup upon encountering the pup following sham or light stimulation. Error bars: ± SEM. Mixed-effects analysis followed with multiple comparisons test. ***p < 0.001, ****p < 0.0001. n = 5 mice for ChR2 virgin group, n = 4 mice for ChR2 mother group.

See Source Data Extended Data Fig. 5 for detailed values and statistics.

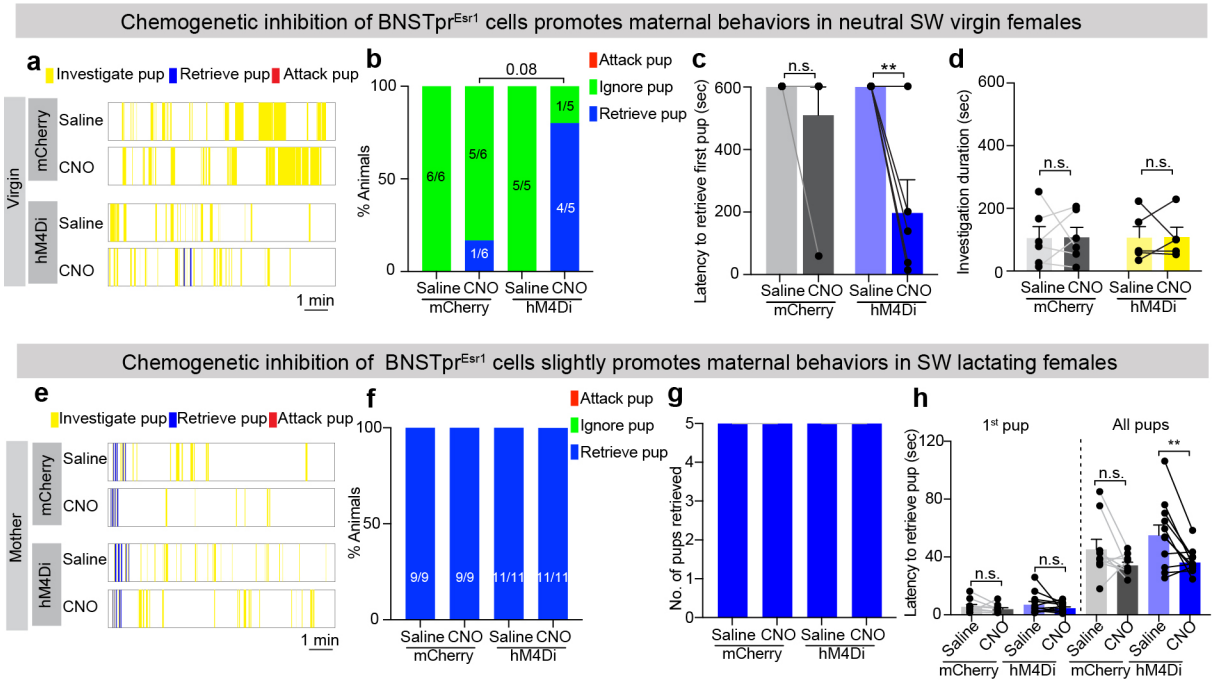

Extended Data Fig. 6: Chemogenetic inhibition of BNSTpr^{Esr1} neurons promotes maternal behavior in non-hostile virgin females and mothers

(a) Representative raster plots showing pup-directed behaviors in non-hostile non-maternal mCherry and hM4Di virgin females after saline or CNO injection.

(b) Percentage of mCherry and hM4Di virgin females that ignore, retrieve or attack pups after saline or CNO injection. Fisher's exact test between mCherry and hM4Di group.

(c, d) Latency to retrieve pup (**c**) and pup investigation duration (**d**) after saline or CNO injection in non-hostile non-maternal virgin mCherry and hM4Di females. Error bars: ± SEM. n = 6 mice for mCherry group; n = 5 mice for hM4Di group. Mixed-effects analysis followed with multiple comparisons test. **p < 0.01.

(e) Representative raster plots showing various pup-directed behaviors in lactating mCherry and hM4Di females after saline or CNO injection.

(f) All mCherry and hM4Di lactating females retrieved pups after saline or CNO injection.

(g) All 5 pups were retrieved in the 10-min testing period in mCherry and hM4Di lactating females after either saline or CNO injection. n = 9 mice for mCherry group; n = 11 mice for hM4Di group.

(h) Latency to retrieve the first pup and all five pups in mCherry and hM4Di lactating females after saline or CNO injection. Error bars: SEM. n = 9 mice for mCherry group; n = 11 mice for hM4Di group. Mixed-effects analysis followed with multiple comparisons test. **p < 0.01.

See Source Data Extended Data Fig. 6 for detailed values and statistics.

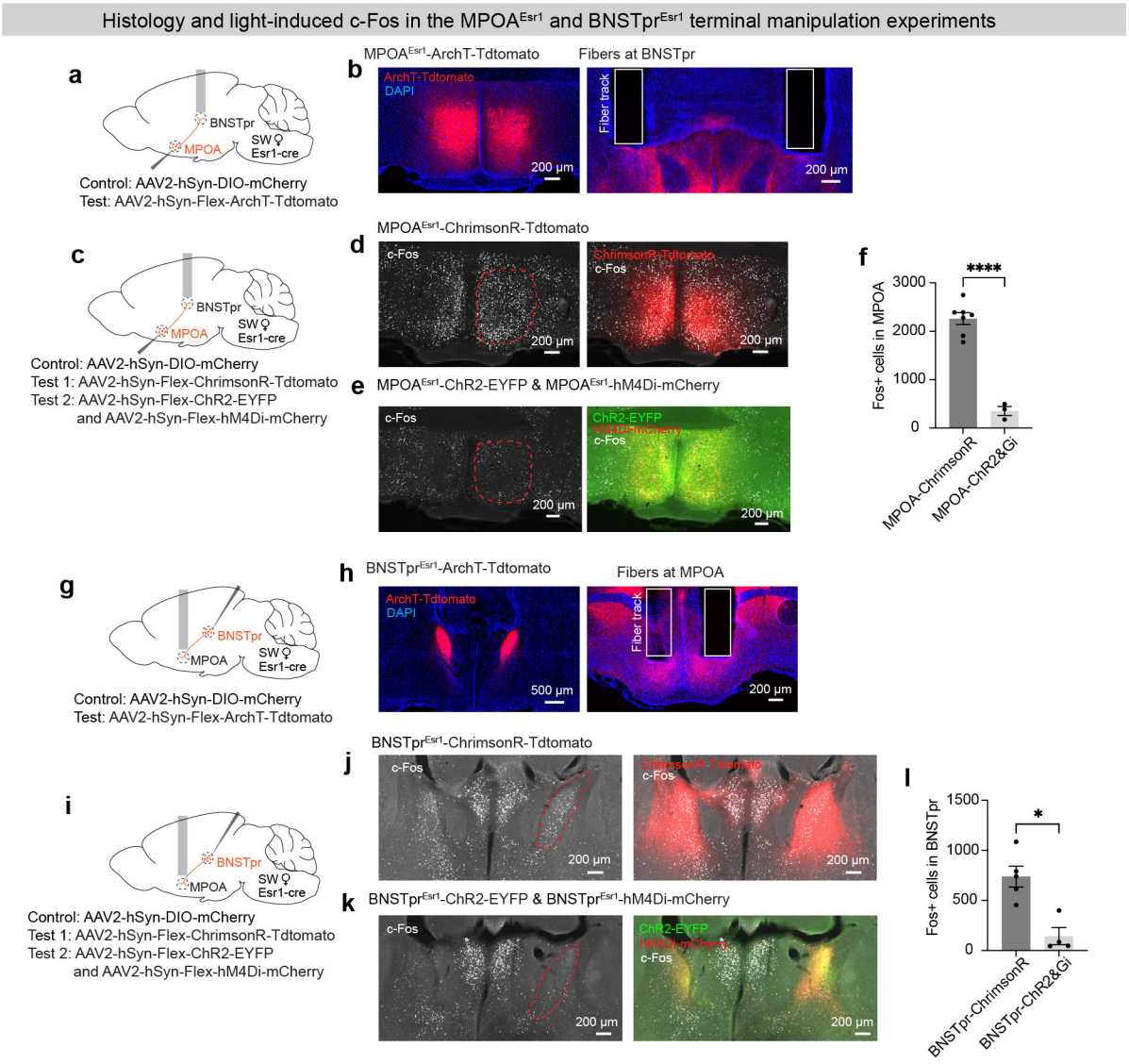

Extended Data Fig. 7: Histology and light-induced c-Fos in the MPOA^{Esr1} and BNSTpr^{Esr1} terminal manipulation experiments

(a) Experimental design to optogenetically inactivate MPOA^{Esr1} inputs to BNSTpr.

(b) Representative histology of 6 mice showing ArchT expression (red) in the MPOA (left), and ArchT expression terminals and optic fiber tracks in the BNSTpr (right).

(c) Experimental design to optogenetically activate MPOA^{Esr1} inputs to the BNSTpr.

(d) Representative histology of 7 mice showing ChrimsonR (red) and c-Fos (white) in the MPOA after delivering 5 mW pulsed yellow light to the right side of the BNSTpr for 10 min.

(e) Representative histology of 3 mice showing ChR2 (green), hM4Di (red), and c-Fos (white) in the MPOA after delivering 10 min 5 mW pulsed blue light to the right side of the BNSTpr 30 min after CNO injection.

(f) Number of c-Fos+ cells in the right MPOA in ChrimsonR and ChR2+Gi group. Error bars: ± SEM. Unpaired t test, ****p<0.0001. n =7 mice for ChrimsonR group, n =3 for ChR2+Gi group.

(g) Experimental design to optogenetically inactivate BNSTpr^{Esr1} inputs to MPOA.

(h) Representative histology of 6 mice showing ArchT (red) in the BNSTpr (left), and ArchT expressing axons and optic fiber tracks in the MPOA (right).

(i) Experimental design to optogenetically activate BNSTpr^{Esr1} inputs to MPOA.

(j) Representative histology of 5 mice showing ChrimsonR (red) and c-Fos (white) in the BNSTpr after delivering 5 mW pulsed yellow light to the right side of the MPOA for 10 min.

(k) Representative histology of 4 mice showing ChR2 (green), hM4Di (red) and c-Fos (white) in BNSTpr after delivering 10 min 5 mW pulsed blue light to the right MPOA 30 min after CNO injection.

(l) Number of c-Fos+ cells in the right BNSTpr in ChrimsonR and ChR2+Gi group. Error bars: ± SEM. Mann Whitney test, *p<0.05. n =5 mice for ChrimsonR group, n =4 for ChR2+Gi group.

See Source Data Extended Data Fig. 7 for detailed values and statistics.

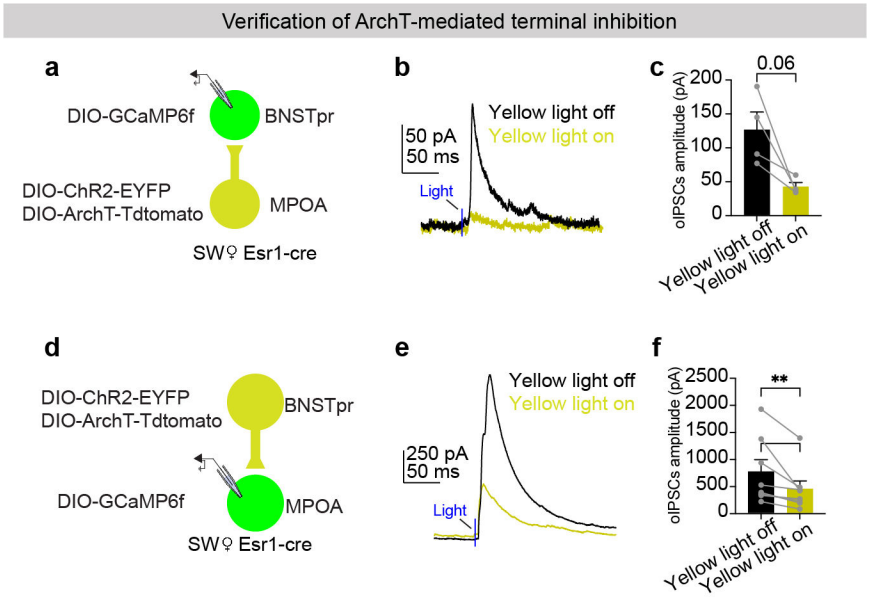

Extended Data Fig. 8: Verification of ArchT-mediated terminal inhibition

(a and d) Experimental design to examine the efficacy of ArchT-mediated inhibition of MPOA^{Esr1} → BNSTpr^{Esr1} (**a**) and BNSTpr^{Esr1} → MPOA^{Esr1} (**d**) projections.

(b and e) Representative blue light pulse evoked IPSCs from BNSTpr^{Esr1} (**b**) and MPOA^{Esr1}cells (**e**) with (yellow) and without (black) simultaneous 5 mW yellow light delivery.

(c and f) The amplitude of oIPSCs of BNSTpr^{Esr1} (**c**) and MPOA^{Esr1}cells (**f**) with and without 5 mW yellow light delivery. Error bars: ± SEM. Paired t-test (**c**) and Wilcoxon matched-pairs signed rank test (**f**), **p<0.01. n = 4 BNSTpr^{Esr1} cells, n = 8 MPOA^{Esr1} cells.

See Source Data Extended Data Fig. 8 for detailed values and statistics.

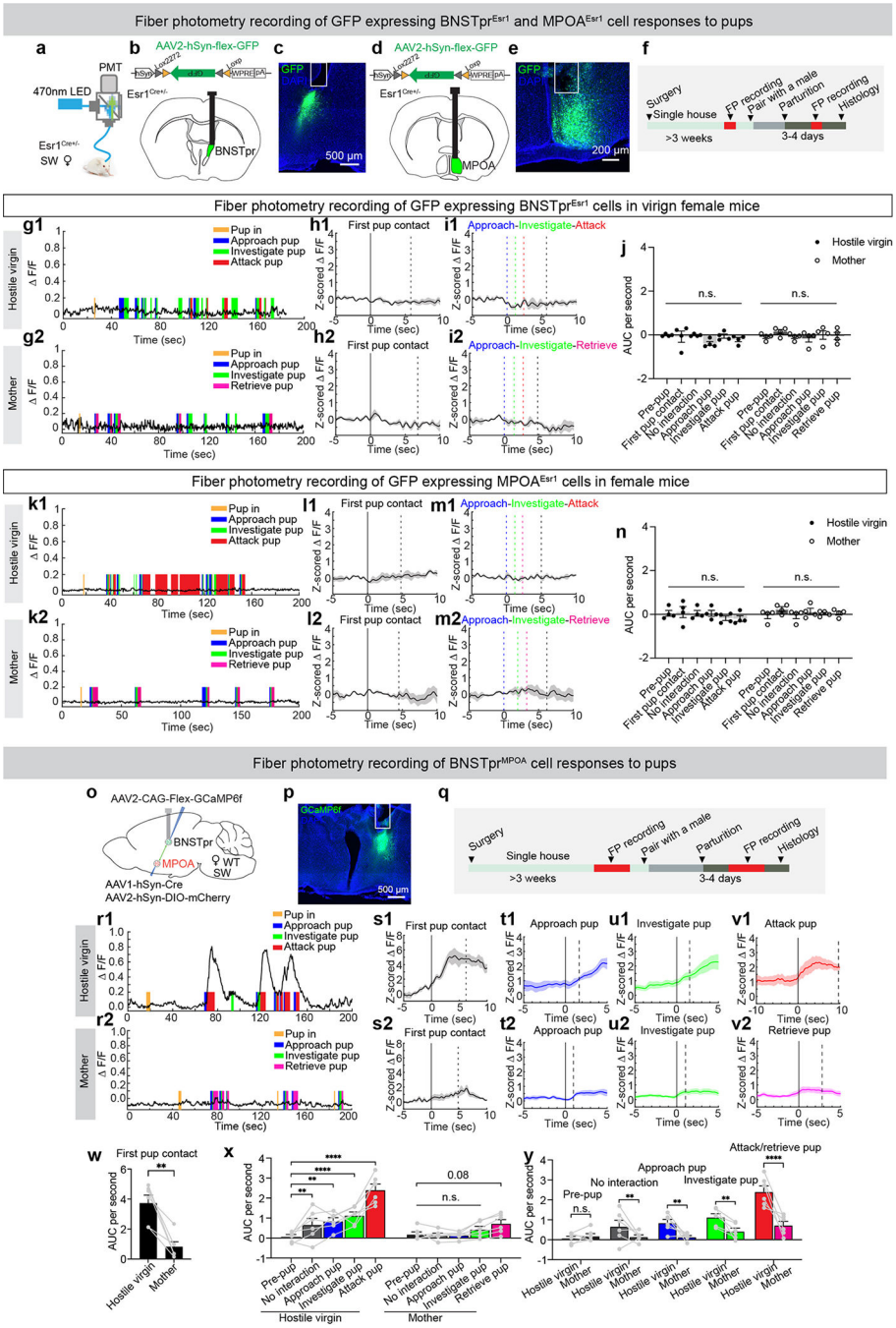

Extended Data Fig. 9: Fiber photometry recording of GFP-expressing BNSTpr^{Esr1} and MPOA^{Esr1} cells and GCaMP6f-expressing BNSTpr^{MPOA} cells during pup interaction

(a) Fiber photometry setup.

(**b and d**) Viral construct and targeted brain regions. Brain illustrations are produced based on reference atlas from https://atlas.brain-map.org/.

(c and e) Representative histological images of 4 mice showing GFP (green) expression and fiber tracks (white box) in BNSTpr (**c**) and MPOA (**e**).

(f) Experimental timeline.

(g, k) Representative GFP recording (ΔF/F) traces of BNSTpr^{Esr1} (**g**) and MPOA^{Esr1} (**k**) cells during pup interaction in a hostile SW virgin female (**g1, k1**) and a mother (**g2, k2**). Color shades indicate various behaviors.

(h, l) PETHs of GFP signal (Z-scored ΔF/F) of BNSTpr^{Esr1} (**h**) and MPOA^{Esr1} (**l**) cells aligned to the first pup contact in hostile virgin females (**h1, l1**), and mothers (**h2, l2**). n = 4 mice. Solid lines indicate the onset on first pup contact; dashed black lines indicate the mean duration of first pup contact. Shades: ± SEM.

(i, m) PETHs of GFP signal (Z-scored ΔF/F) of BNSTpr^{Esr1} (**i**) and MPOA^{Esr1} (**m**) cells aligned to the onset of pup approach in hostile virgin females **(i1, m1**), and mothers (**i2, m2**). n = 4 mice for each group. Blue dashed lines indicate the onset of pup approach; green dashed lines indicate the mean latency to pup investigation; the red and black dashed lines in **i1** and **m1** indicate the mean latency to attack and stop attacking pups, respectively; the magenta and black dashed lines in **i2** and **m2** indicate the mean latency to retrieve and stop retrieving pups, respectively. Shades: ± SEM.

(j, n) Mean AUC of Z-scored ΔF/F signal of BNSTpr^{Esr1} (**j**) and MPOA^{Esr1} (**n**) cells during various pup-directed behaviors in hostile virgin females and mothers. Two-way RM ANOVA (**j**) and Mixed-effects analysis (**n**) followed with multiple comparisons test. n = 4 mice for each group. Error bars: ± SEM.

(o) Experimental design.

(p) A representative histological image of 9 mice showing GCaMP6f (green) expression and the fiber track in BNSTpr (white lines).

(q) Experimental timeline.

(r) Representative GCaMP6f recording (ΔF/F) traces of BNSTpr^{MPOA} cells during pup interaction in a hostile SW virgin female (**r1**) and a mother (**r2**). Color shades indicate various behaviors.

(s-v) PETHs of GCaMP6f signal (Z-scored ΔF/F) of BNSTpr^{MPOA} cells aligned to the onset of various behaviors in hostile virgin females **(s1-v1**), and mothers (**s2-v2**). n = 6 mice. Solid lines indicate the onset on each behavior; dashed black lines indicate the end of each behavior. Shades: ± SEM.

(w) Mean AUC of Z-scored ΔF/F signal of BNSTpr^{MPOA} cells during the first pup contact. Paired t-test. **p < 0.01. Error bars: SEM. n = 6 mice.

(x, y) Mean AUC of Z-scored ΔF/F signal of BNSTpr^{MPOA} cells during pre-pup period and various pup-directed behaviors in hostile virgin females and mothers. Two-way RM ANOVA followed with multiple comparisons test. **p < 0.01, ****p < 0.0001, mean ± SEM. n = 6 mice.

See Source Data Extended Data Fig. 9 for detailed values and statistics.

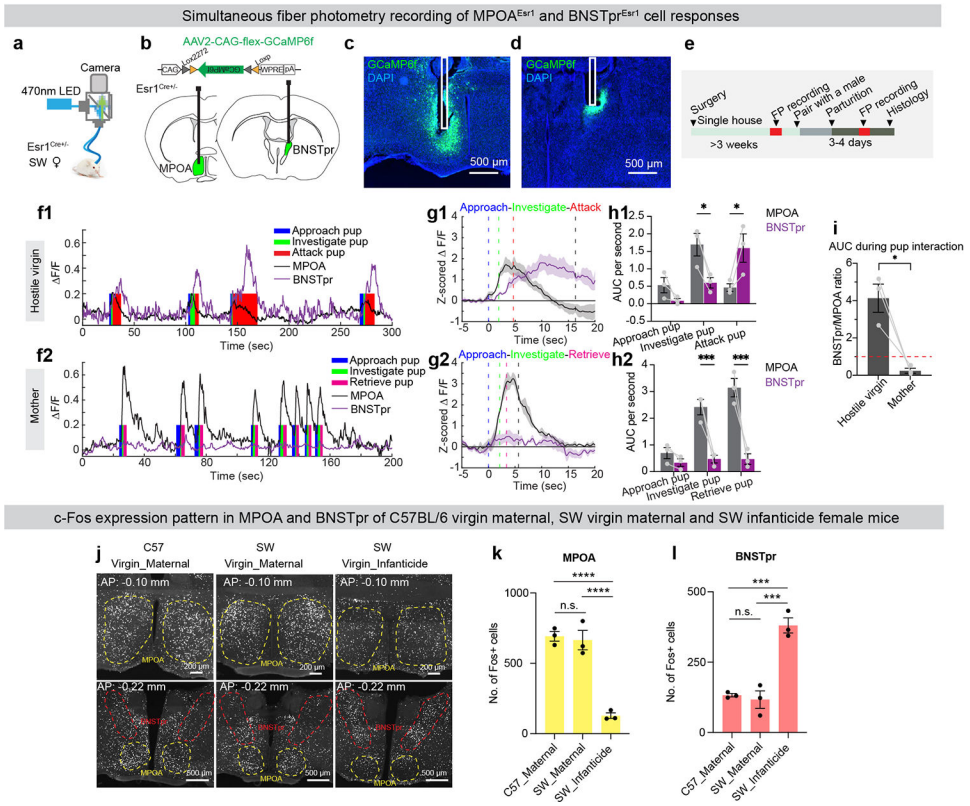

Extended Data Fig. 10: Simultaneous recording of MPOA^{Esr1} and BNSTpr^{Esr1} cells and comparing infanticide and maternal behavior-induced c-Fos between strains.

(a) Fiber photometry setup.

(**b**) Viral construct and targeted brain regions. Brain illustrations are produced based on reference atlas from https://atlas.brain-map.org/.

(c, d) Representative histological images of 3 mice showing GCaMP6f (green) expression and fiber tracks (white boxes) in MPOA (**c**) and BNSTpr (**d**).

(e) Experimental timeline.

(f) Representative GCaMP6f recording (ΔF/F) traces of MPOA^{Esr1} (black) and BNSTpr^{Esr1} (purple) cells during pup interaction in a hostile SW virgin female (**f1**) and a mother (**f2**). Color shades indicate various behaviors.

(g) PETHs of GCaMP6f signal (Z-score ΔF/F) of MPOA^{Esr1} (black) and BNSTpr^{Esr1} (purple) cells aligned to the onset of pup approach in hostile virgin females **(g1)**, and mothers (**g2**). n = 3 mice for each group. Blue dashed lines indicate the onset of pup approach; green dashed lines indicate the mean latency to pup investigation; the red and black dashed lines in **g1** indicate the mean latency to attack and stop attacking pups, respectively; the magenta and black dashed lines in **g2** indicate the mean latency to retrieve and stop retrieving pups, respectively. Shades: ± SEM.

(h) Mean AUC of Z-scored ΔF/F signal of MPOA^{Esr1} (black) and BNSTpr^{Esr1} (purple) cells during pup approach, investigation, attack, and retrieval in hostile virgin females (**h1**) and mothers (**h2**). Two-way RM ANOVA (**h1**) and Mixed-effects analysis (**h2**) followed with multiple comparisons test. n = 3 mice for each group, *p < 0.05, ***p < 0.001, mean ± SEM.

(i) BNSTpr^{Esr1} and MPOA^{Esr1} response ratio in hostile virgin females and mothers during pup interaction period. The red dashed line indicates 1. n = 3 mice for each group, Paired *t-test*. *p < 0.05, mean ± SEM.

(j) Representative histological images of 3 mice in each group showing c-Fos expression in MPOA and BNSTpr of a C57BL/6 virgin maternal female (left), a SW virgin maternal female (middle), and a SW infanticidal female (right).

(k, l) Number of c-Fos+ cells in MPOA (**k**) and BNSTpr (**l**) in C57BL/6 virgin maternal, SW virgin maternal and SW infanticidal female mice. n=3 for each group, ***p < 0.001, ****p < 0.0001. Error bars: ± SEM. One-way ANOVA followed with multiple comparisons test.

See Source Data Extended Data Fig. 10 for detailed values and statistics.

Supplementary Material

Refer to Web version on PubMed Central for supplementary material.

Acknowledgements

We thank all the Lin lab members for inspiring discussion, and Yiwen Jiang for assisting with genotyping. This research was supported by NIH grants 1R01HD092596 (D.L. and R.S.), R01MH101377, R01MH124927 and U19NS107616 (D.L.), the Mathers Foundation, and the Vulnerable Brain Project (D.L.), and the Levy Leon Postdoctoral Fellowship (M.L.).

Data Availability

Raw values associated with each figure panel can be found in the source data files.

Fiber photometry recording data, behavior annotations and raw representative histology images can be downloaded from 10.5281/zenodo.7772552. Behavior videos and additional histology images are available from the corresponding author upon reasonable request.

References

1. Parmigiani S & vom Saal F Infanticide And Parental Care. (2016).
2. Dulac C, O'Connell LA & Wu Z Neural control of maternal and paternal behaviors. Science 345, 765–770, doi:10.1126/science.1253291 (2014). [PubMed: 25124430]
3. Soroker V & Terkel J Changes in incidence of infanticidal and parental responses during the reproductive cycle in male and female wild mice Mus musculus. Animal Behaviour 36, 1275–1281 (1988).
4. McCarthy MM & vom Saal FS The influence of reproductive state on infanticide by wild female house mice (Mus musculus). Physiology & behavior 35, 843–849 (1985). [PubMed: 3912779]
5. Kohl J, Autry AE & Dulac C The neurobiology of parenting: A neural circuit perspective. Bioessays 39, 1–11, doi:10.1002/bies.201600159 (2017).
6. Numan M Motivational systems and the neural circuitry of maternal behavior in the rat. Dev Psychobiol 49, 12–21, doi:10.1002/dev.20198 (2007). [PubMed: 17186513]
7. Kohl J & Dulac C Neural control of parental behaviors. Curr Opin Neurobiol 49, 116–122, doi:10.1016/j.conb.2018.02.002 (2018). [PubMed: 29482085]
8. Yu Z-X, Li X-Y & Xu X-H Neural Circuit Mechanisms That Underlie Parental Care. Neural Circuits of Innate Behaviors, 49–62 (2020).
9. Numan M & Insel TR The neurobiology of parental behavior. (Springer, 2003).
10. Kuroda KO & Numan M The medial preoptic area and the regulation of parental behavior. Neurosci Bull 30, 863–865, doi:10.1007/s12264-014-1462-z (2014). [PubMed: 25096498]

11. Carollo A, Balagtas JPM, Neoh MJ & Esposito G A Scientometric Approach to Review the Role of the Medial Preoptic Area (MPOA) in Parental Behavior. Brain Sci 11, doi:10.3390/brainsci11030393 (2021).
12. Lukas D & Huchard E The evolution of infanticide by females in mammals. Philosophical Transactions of the Royal Society B: Biological Sciences 374, 20180075, doi:10.1098/rstb.2018.0075 (2019).
13. Palombit RA Infanticide as sexual conflict: coevolution of male strategies and female counterstrategies. Cold Spring Harb Perspect Biol 7, a017640, doi:10.1101/cshperspect.a017640 (2015). [PubMed: 25986557]
14. Jakubowski M & Terkel J Infanticide and caretaking in non-lactating Mus musculus: influence of genotype, family group and sex. Animal Behaviour 30, 1029–1035 (1982).
15. Svare B & Mann M Infanticide: genetic, developmental and hormonal influences in mice. Physiology & behavior 27, 921–927, doi:10.1016/0031-9384(81)90062-7 (1981). [PubMed: 7323200]
16. Gandelman R The ontogeny of maternal responsiveness in female Rockland-Swiss albino mice. Hormones and Behavior 4, 257–268, doi:10.1016/0018-506X(73)90010-X (1973). [PubMed: 4785736]
17. Wei YC et al. Medial preoptic area in mice is capable of mediating sexually dimorphic behaviors regardless of gender. Nature communications 9, 279, doi:10.1038/s41467-017-02648-0 (2018).
18. Fang YY, Yamaguchi T, Song SC, Tritsch NX & Lin D A Hypothalamic Midbrain Pathway Essential for Driving Maternal Behaviors. Neuron 98, 192–207.e110, doi:10.1016/j.neuron.2018.02.019 (2018). [PubMed: 29621487]
19. Wu Z, Autry AE, Bergan JF, Watabe-Uchida M & Dulac CG Galanin neurons in the medial preoptic area govern parental behaviour. Nature 509, 325–330, doi:10.1038/nature13307 (2014). [PubMed: 24828191]
20. Kohl J et al. Functional circuit architecture underlying parental behaviour. Nature 556, 326–331, doi:10.1038/s41586-018-0027-0 (2018). [PubMed: 29643503]
21. Tsuneoka Y et al. Neurotransmitters and neuropeptides in gonadal steroid receptor-expressing cells in medial preoptic area subregions of the male mouse. Sci Rep 7, 9809, doi:10.1038/s41598-017-10213-4 (2017). [PubMed: 28852050]
22. Li XY et al. AGRP Neurons Project to the Medial Preoptic Area and Modulate Maternal Nest-Building. J Neurosci 39, 456–471, doi:10.1523/JNEUROSCI.0958-18.2018 (2019). [PubMed: 30459220]
23. Zhang G-W et al. Medial preoptic area antagonistically mediates stress-induced anxiety and parental behavior. Nature neuroscience, doi:10.1038/s41593-020-00784-3 (2021).
24. Tsuneoka Y et al. Distinct preoptic-BST nuclei dissociate paternal and infanticidal behavior in mice. The EMBO journal 34, 2652–2670, doi:10.15252/embj.201591942 (2015). [PubMed: 26423604]
25. Autry AE et al. Urocortin-3 neurons in the mouse perifornical area promote infant-directed neglect and aggression. Elife 10, doi:10.7554/eLife.64680 (2021).
26. Sato K et al. Amygdalohippocampal area neurons that project to the preoptic area mediate infant-directed attack in male mice. Journal of Neuroscience 40, 3981–3994 (2020). [PubMed: 32284340]
27. Chen PB et al. Sexually Dimorphic Control of Parenting Behavior by the Medial Amygdala. Cell, doi:10.1016/j.cell.2019.01.024 (2019).
28. Numan M Medial preoptic area and maternal behavior in the female rat. Journal of comparative and physiological psychology 87, 746–759, doi:10.1037/h0036974 (1974). [PubMed: 4426995]
29. Numan M, Corodimas KP, Numan MJ, Factor EM & Piers WD Axon-sparing lesions of the preoptic region and substantia innominata disrupt maternal behavior in rats. Behavioral neuroscience 102, 381 (1988). [PubMed: 3395448]
30. Mann MA, Kinsley C, Broida J & Svare B Infanticide exhibited by female mice: genetic, developmental and hormonal influences. Physiology & behavior 30, 697–702 (1983). [PubMed: 6878475]

31. Zingg B et al. AAV-Mediated Anterograde Transsynaptic Tagging: Mapping Corticocollicular Input-Defined Neural Pathways for Defense Behaviors. Neuron 93, 33–47, doi:10.1016/j.neuron.2016.11.045 (2017). [PubMed: 27989459]
32. Madisen L et al. A robust and high-throughput Cre reporting and characterization system for the whole mouse brain. Nature neuroscience 13, 133–140, doi:10.1038/nn.2467 (2010). [PubMed: 20023653]
33. Chen A-X et al. Specific Hypothalamic Neurons Required for Sensing Conspecific Male Cues Relevant to Inter-male Aggression. Neuron, doi:10.1016/j.neuron.2020.08.025 (2020).
34. Stagkourakis S et al. A neural network for intermale aggression to establish social hierarchy. Nature neuroscience 21, 834–842, doi:10.1038/s41593-018-0153-x (2018). [PubMed: 29802391]
35. Gallo M et al. Limited Bedding and Nesting Induces Maternal Behavior Resembling Both Hypervigilance and Abuse. Front Behav Neurosci 13, 167, doi:10.3389/fnbeh.2019.00167 (2019). [PubMed: 31402857]
36. Nephew BC & Bridges RS Effects of chronic social stress during lactation on maternal behavior and growth in rats. Stress 14, 677–684, doi:10.3109/10253890.2011.605487 (2011). [PubMed: 21875305]
37. Kim SY et al. Diverging neural pathways assemble a behavioural state from separable features in anxiety. Nature 496, 219–223, doi:10.1038/nature12018 (2013). [PubMed: 23515158]
38. Jennings JH et al. Distinct extended amygdala circuits for divergent motivational states. Nature 496, 224–228, doi:10.1038/nature12041 (2013). [PubMed: 23515155]
39. Lebow MA & Chen A Overshadowed by the amygdala: the bed nucleus of the stria terminalis emerges as key to psychiatric disorders. Mol Psychiatry 21, 450–463, doi:10.1038/mp.2016.1 (2016). [PubMed: 26878891]
40. Mitra SW et al. Immunolocalization of estrogen receptor beta in the mouse brain: comparison with estrogen receptor alpha. Endocrinology 144, 2055–2067, doi:10.1210/en.2002-221069 (2003). [PubMed: 12697714]
41. Lee H et al. Scalable control of mounting and attack by Esr1+ neurons in the ventromedial hypothalamus. Nature 509, 627–632, doi:10.1038/nature13169 (2014). [PubMed: 24739975]
42. Hashikawa K et al. Esr1(+) cells in the ventromedial hypothalamus control female aggression. Nat Neurosci 20, 1580–1590, doi:10.1038/nn.4644 (2017). [PubMed: 28920934]
43. Yamaguchi T et al. Posterior amygdala regulates sexual and aggressive behaviors in male mice. Nat Neurosci, doi:10.1038/s41593-020-0675-x (2020).
44. Kelly DA, Varnum MM, Krentzel AA, Krug S & Forger NG Differential control of sex differences in estrogen receptor α in the bed nucleus of the stria terminalis and anteroventral periventricular nucleus. Endocrinology 154, 3836–3846, doi:10.1210/en.2013-1239 (2013). [PubMed: 24025225]
45. Fang YY, Yamaguchi T, Song SC, Tritsch NX & Lin D A Hypothalamic Midbrain Pathway Essential for Driving Maternal Behaviors. Neuron 98, 192–207 e110, doi:10.1016/j.neuron.2018.02.019 (2018). [PubMed: 29621487]
46. Nguyen AQ, Dela Cruz JA, Sun Y, Holmes TC & Xu X Genetic cell targeting uncovers specific neuronal types and distinct subregions in the bed nucleus of the stria terminalis. J Comp Neurol 524, 2379–2399, doi:10.1002/cne.23954 (2016). [PubMed: 26718312]
47. Hrdy SB Infanticide among animals: a review, classification, and examination of the implications for the reproductive strategies of females. Ethology and Sociobiology 1, 13–40 (1979).
48. Knoedler JR et al. A functional cellular framework for sex and estrous cycle-dependent gene expression and behavior. Cell 185, 654–671 e622, doi:10.1016/j.cell.2021.12.031 (2022). [PubMed: 35065713]
49. Yang B, Karigo T & Anderson DJ Transformations of neural representations in a social behaviour network. Nature 608, 741–749, doi:10.1038/s41586-022-05057-6 (2022). [PubMed: 35922505]
50. Zhou X et al. Hyperexcited limbic neurons represent sexual satiety and reduce mating motivation. Science 379, 820–825, doi:10.1126/science.abl4038 (2023). [PubMed: 36758107]

Method-only references

51. Mathis A et al. DeepLabCut: markerless pose estimation of user-defined body parts with deep learning. Nature neuroscience 21, 1281–1289, doi:10.1038/s41593-018-0209-y (2018). [PubMed: 30127430]
52. Yin L et al. VMHvllCckar cells dynamically control female sexual behaviors over the reproductive cycle. Neuron (2022).
53. Yin L et al. VMHvll(Cckar) cells dynamically control female sexual behaviors over the reproductive cycle. Neuron, doi:10.1016/j.neuron.2022.06.026 (2022).
54. Yamaguchi T et al. Posterior amygdala regulates sexual and aggressive behaviors in male mice. Nat Neurosci 23, 1111–1124, doi:10.1038/s41593-020-0675-x (2020). [PubMed: 32719562]
55. Wong LC et al. Effective Modulation of Male Aggression through Lateral Septum to Medial Hypothalamus Projection. Curr Biol 26, 593–604, doi:10.1016/j.cub.2015.12.065 (2016). [PubMed: 26877081]
56. Falkner AL et al. Hierarchical Representations of Aggression in a Hypothalamic-Midbrain Circuit. Neuron 106, 637–648 e636, doi:10.1016/j.neuron.2020.02.014 (2020). [PubMed: 32164875]

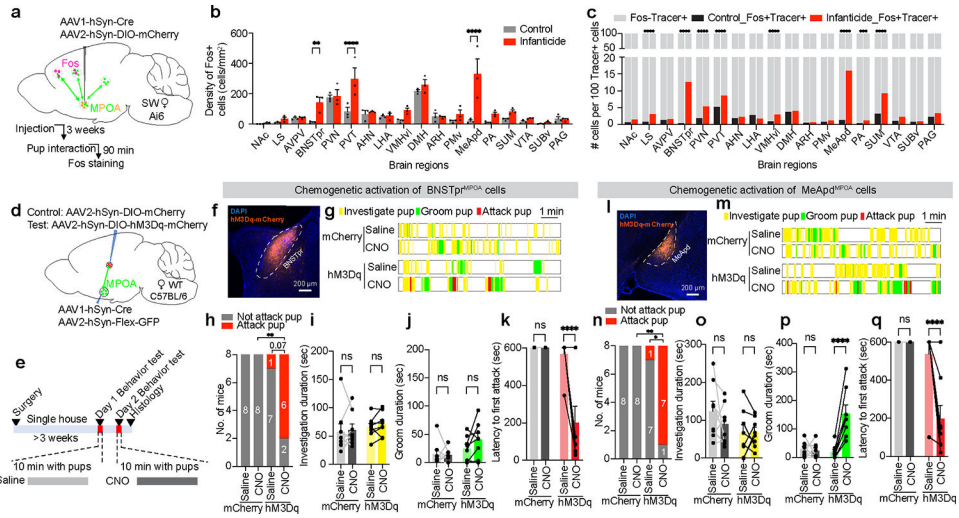

Fig. 1: Functional screening of brain regions relevant for negative pup-directed behaviors in females

(a) Experimental design to identify infanticide-activated MPOA-connecting cells in female mice.

(b) The density of c-Fos expressing cells in MPOA-connecting brain regions in female mice after infanticide or left undisturbed (control). n = 3 mice/group.

(c) Total number of Fos+Tracer+ and Fos-Tracer+ cells per 100 Tracer+ cells in MPOA-connecting brain regions across all infanticide and control females.

(d) Experimental design to chemogenetically activate MPOA-connecting brain regions.

(e) Experimental timeline.

(f) Representative histology images showing hM3Dq-mCherry expression (red) in BNSTpr^{MPOA} cells. Blue: DAPI.

(g) Representative raster plots showing pup-directed behaviors after saline or CNO injection in mCherry and hM3Dq mice.

(h) The number of female mice that attack or not after saline or CNO injection in mCherry and hM3Dq mice.

(i-k) Investigating pup duration (**i**), grooming pup duration (**j**), and latency to attack pups (**k**) after saline or CNO injection in mCherry and hM3Dq mice. Each line represents one animal. If no behavior of interest is observed during the test, the latency is 600 s.

(l-q) Chemogenetic activation of MeApd^{MPOA} cells increases infanticide and pup grooming. Figure conventions as in **f-k**.

All error bars: SEM. **(c)** Fisher's exact test based on raw Fos+Tracer+ and Fos-Tracer+ cell numbers for each brain region. (**h, n**) McNemar's test for saline vs. CNO comparison. Fisher's exact test for mCherry vs. hM3Dq compraison. Two-way RM ANOVA (**b, I, o, p**), or Mixed-effects analysis (**j, k, q**) followed with multiple comparisons test. All tests are two-sided. **p < 0.01; ***p < 0.001; ****p < 0.0001. See Source Data Fig. 1 for detailed values and statistics for all plots.

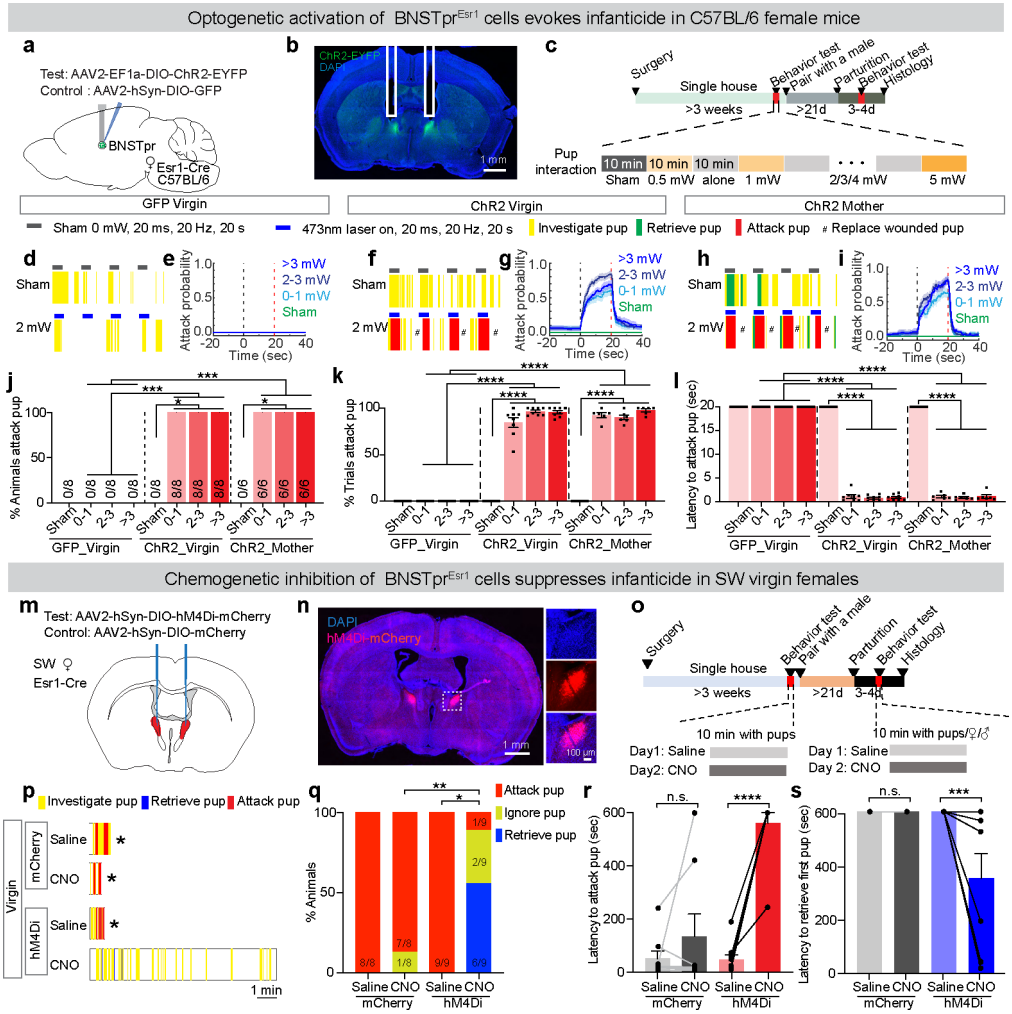

Fig. 2: BNSTpr^{Esr1} neurons are sufficient and necessary for female infanticide.

(a) Experimental design.

(b) Representative histology showing ChR2-EYFP expression. White lines: fiber tracks.

(c) Experimental timeline.

(d, f, h) Raster plots showing pup-directed behaviors during sham and light stimulation. # Replace a pup.

(e, g, i) Post-event histograms (PETHs) of attack pup probability aligned to sham and light onset. Only trials with female-pup contact were included. Dashed lines mark light period.

(j) Percentage of animals that attacked pups.

(k) Percentage of trials showing pup attack. Only trials with female-pup contact were included.

(l) Average latency to attack pup upon pup encounter following sham or light stimulation.

(m) Experimental design to inhibit BNSTpr^{Esr1} cells. Brain illustration is based on reference atlas from https://atlas.brain-map.org/.

(n) Representative histology showing hM4Di-mCherry expression.

(o) Experimental timeline.

(p) Raster plots showing pup-directed behaviors after CNO or saline injection. *Remove wounded pups and stop recording.
(q) Percentage of spontaneously infanticidal virgin females that attack, ignore or retrieve pups after saline or CNO injection.
(r, s) Latency to attack (**r**) and retrieve pups (**s**) after saline or CNO injection. Latency equals to 600 s if the behavior doesn't occur during the test.
(**k, l, r, s**) Each dot or line represents one animal. Shades in (**e, g, i**) and error bars in (**k, l, r, s**): ±SEM. **(j, q)** Fisher's exact test for between animal comparisons; McNemar's test for within animal comparisons. (**k, l, r, s**) Mixed-effects analysis followed with multiple comparisons test. All tests are two-sided. *p< 0.05, **p<0.01, ***p < 0.001. ****p < 0.0001. (**e, g, i, j-l**) n = 8 (GFP), 8 (ChR2 virgin) and 6 (ChR2 mother) mice. (**q-s**) n = 8 (mCherry) and 9 (hM4Di) mice. See Source Data Fig. 2 for detailed values and statistics.

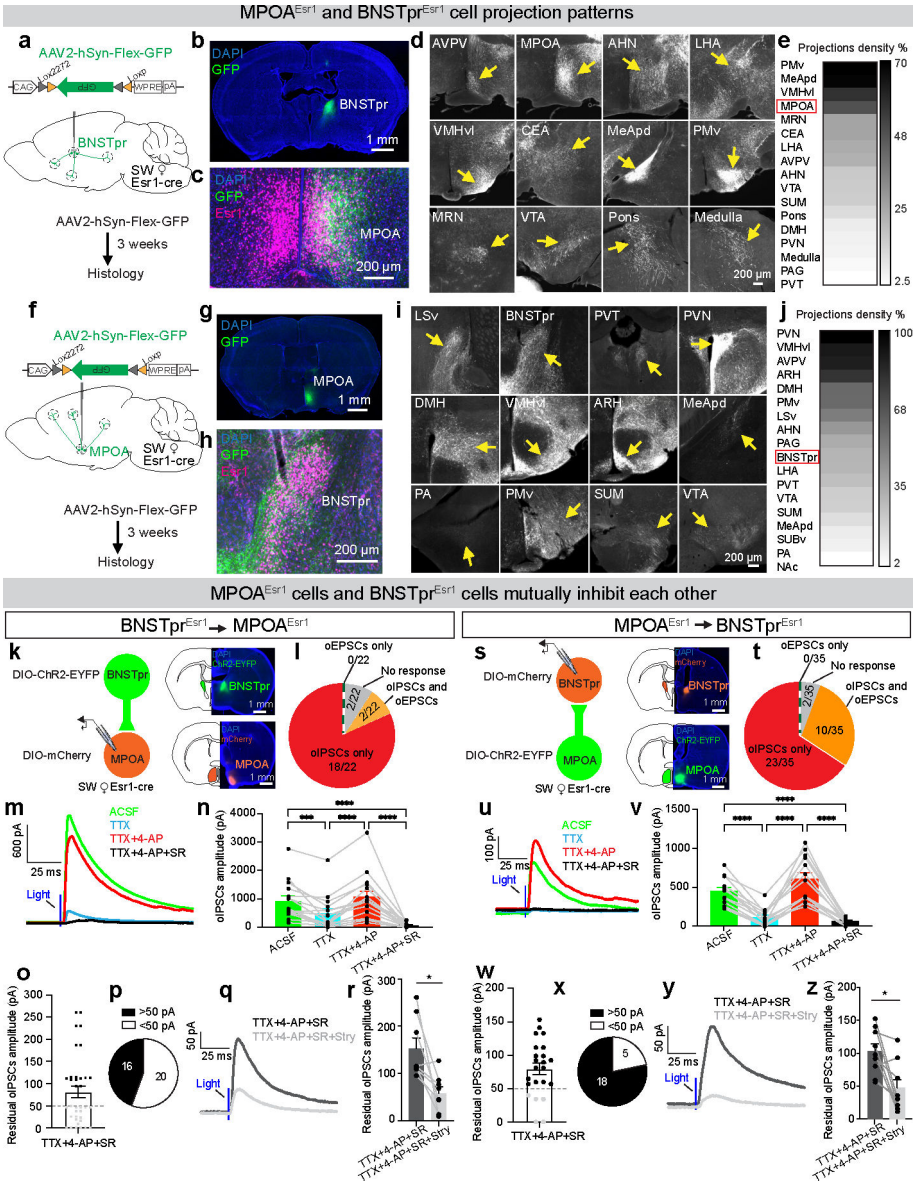

Fig. 3: Mutual inhibition between BNSTpr^{Esr1} and MPOA^{Esr1} cells

(a) Anterograde tracing of BNSTpr^{Esr1} cells. **(b)** Representative GFP expression in BNSTpr^{Esr1} cells.

(c) Representative GFP-expressing BNSTpr^{Esr1} terminals (green) in the MPOA and Esr1 staining (magenta).

(d) Representative GFP-expressing BNSTpr^{Esr1} terminals in various regions.

(e) The brain-wide projection density of BNSTpr^{Esr1} cells, normalized by BNSTpr fluorescence intensity. n = 4 mice.

(f-j) MPOA^{Esr1} cell projection patterns. n = 4 mice. Figure conventions as in **a-e**.

(k, s) Schematics of ChR2-assisted circuit mapping of BNSTpr^{Esr1}→MPOA^{Esr1} (**k**) and MPOA^{Esr1}→BNSTpr^{Esr1} (**s**) pathways and representative histological images. Brain atlas are reproduced based on reference atlas from atlas.brain.org.

(l, t) The synaptic response patterns of MPOA^{Esr1} cells to BNSTpr^{Esr1} terminal activation (**l,** 22 cells/3 mice) and BNSTpr^{Esr1} cells to MPOA^{Esr1} terminal activation (**t**, 35 cells/3 mice).
(m, u) Representative oIPSCs from MPOA^{Esr1} (**m**) and BNSTpr^{Esr1} cells (**u**) with different blockers.
(n, v) oIPSC amplitude with different blockers. Mixed-effects analysis followed with multiple comparisons test. ***p < 0.001, ****p < 0.0001. n = 16 cells/4 mice (**n**); 13 cells/5 mice (**v**).
(o, w) oIPSC amplitude of MPOA^{Esr1} (**o**) and BNSTpr^{Esr1} cells (**w**) after applying TTX, 4-AP, and gabazine mixture. n = 36 cells/8 mice (**o**) and 23 cells/9 mice (**w**).
(p, x) The number of MPOA^{Esr1} (**p**) and BNSTpr^{Esr1} cells (**x**) having a residual oIPSC >50 or <50 pA after applying TTX, 4-AP, and gabazine mixture.
(q, y) Representative oIPSCs of MPOA^{Esr1} (**q**) and BNSTpr^{Esr1} cells (**y**) before and after applying strychnine, a glycine receptor antagonist.
(r, z) Amplitude of oIPSCs of MPOA^{Esr1} (**r**) and BNSTpr^{Esr1} cells (**z**) before and after applying strychnine. Two-sided paired signed rank test, *p<0.05. n = 8 cells/4 mice (**r**); 9 cells/4 mice (**z**). All error bars: SEM.
See Source Data Fig. 3 for detailed values and statistics.

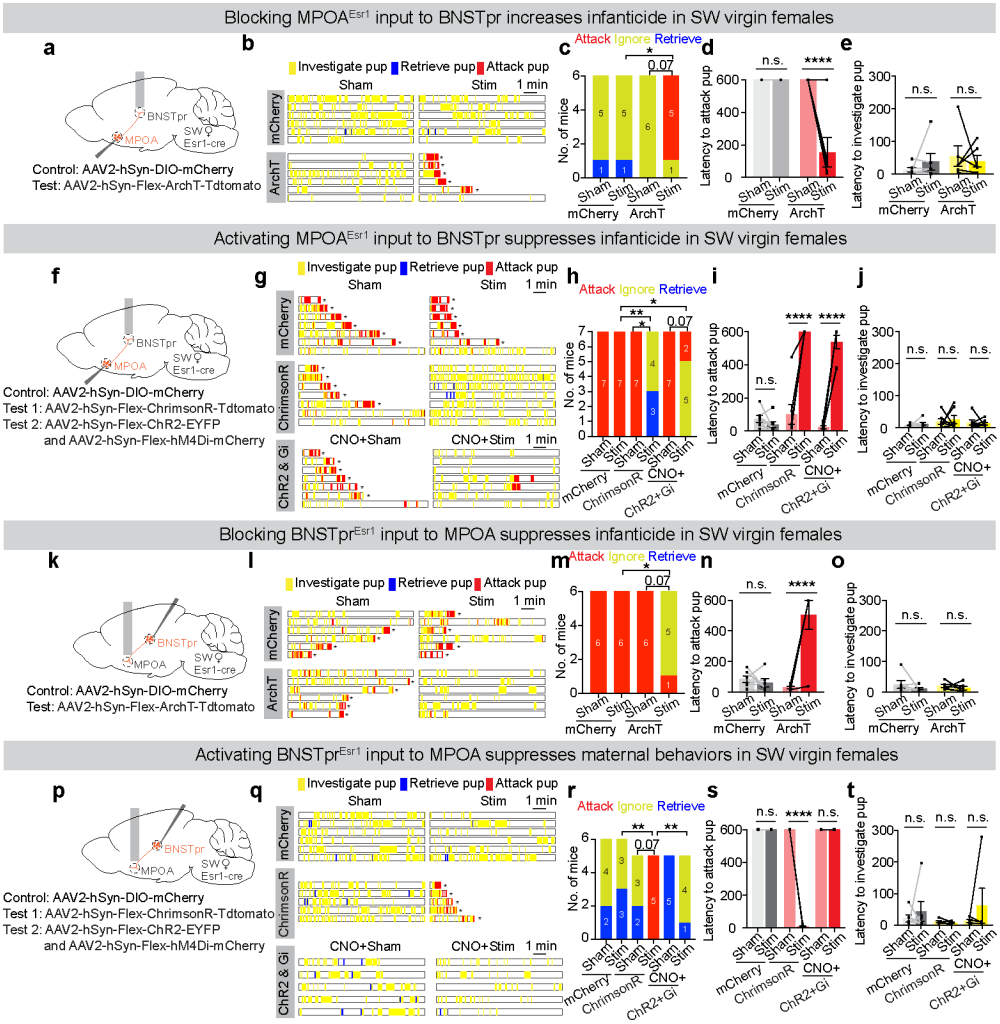

Fig. 4: BNSTpr^{Esr1} and MPOA^{Esr1} cells antagonize each other functionally through their reciprocal projections.

(a) Experimental design to optogenetically inactivate MPOA^{Esr1}→BNSTpr pathway.

(b) Raster plots showing pup-directed behaviors in mCherry and ArchT females during sham or 5 mW continuous yellow light delivery. *Remove wounded pups and stop recording.

(c) Number of mCherry and ArchT females that attack, ignore or retrieve pups during sham or light stimulation.

(d, e) Latency to attack (**d**) and investigate pup (**e**) during sham and light delivery in mCherry and ArchT females. The latency equals to 600s if the behavior of interest doesn't occur during the test. n = 6 mice/group.

(f) Experimental design to optogenetically activate BNSTpr^{Esr1}→MPOA pathway with or without BNSTpr^{Esr1} chemogenetic inhibition.

(g) Raster plots showing pup-directed behaviors in various groups during sham or light delivery. *Remove wounded pups and stop recording.

(h) Number of females in each group that attack, ignore, or retrieve pups during sham or light delivery.

(i, j) Latency to attack (**i**) and investigate pup (**j**) during sham or light delivery in control and test females. n = 7 mice/group.

(k-o) Optogenetic inactivation of BNSTpr^{Esr1}→MPOA pathway in spontaneously infanticidal virgin SW females suppresses infanticide. Figure conventions as in **a-e**. n = 6 mice/group.

(p-t) Optogenetic activation of BNSTpr^{Esr1}→MPOA pathway suppresses maternal behaviors. Figure conventions as in **f-j**. n = 6 (mCherry), 5(ChrimsonR), and 5(ChR2+Gi) mice.

All error bars: ± SEM. (**c, h**) Fisher's exact test for comparing behavior outcomes (attack vs. not attack) between control and test groups with the same light treatment. McNemar's test for comparison between light and sham trials within a group. (**d, e, i, j**) Mixed-effects analysis followed with multiple comparisons test. All tests are two-sided. *p < 0.05; **p < 0.01; ****p < 0.0001. See Source Data Fig. 4 for detailed values and statistics.

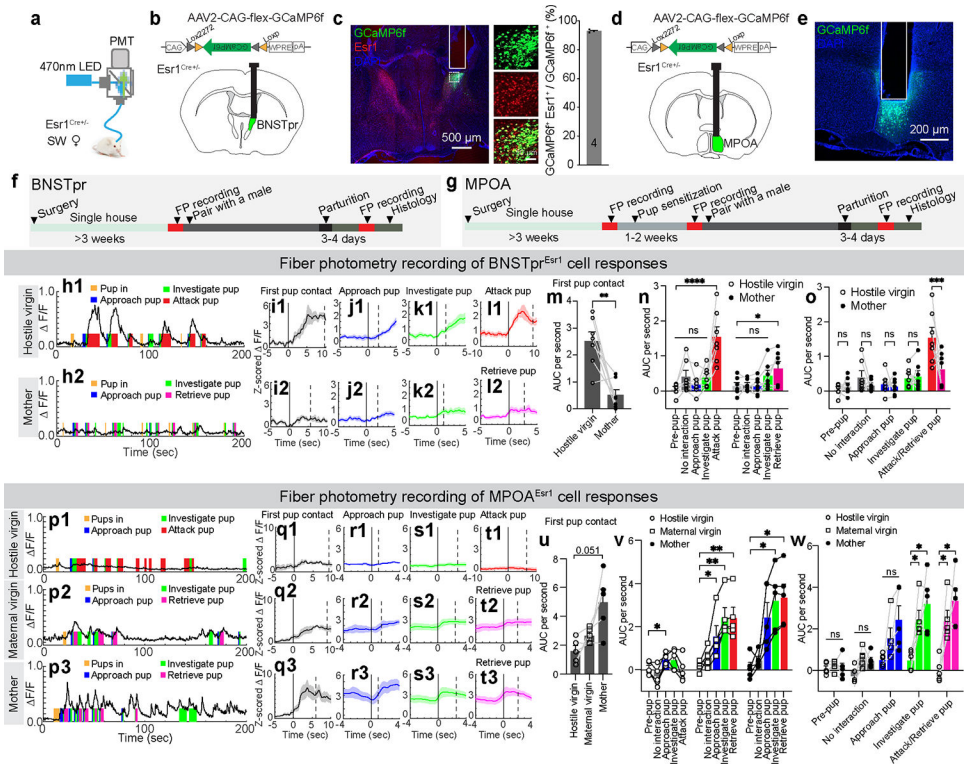

Fig. 5: Distinct responses of BNSTpr^{Esr1} and MPOA^{Esr1} cells during female infanticide and maternal care.

(a) Fiber photometry setup.

(b, d) Viral construct and targeted brain regions. Brain illustration is produced based on reference atlas from https://atlas.brain-map.org/.

(c) A representative image of 4 mice showing the fiber track in BNSTpr (white line), the overlap between Esr1 staining (red) and GCaMP6f (green). Right shows the enlarged view of the boxed area. Bar graph showing the percentage of GCaMP6f cells expressing Esr1. n = 4 recording mice.

(e) Representative GCaMP6f expression (green) and fiber track (white line) in the MPOA of 4 mice.

(f, g) Experimental timelines.

(h) Representative ΔF/F traces of BNSTpr^{Esr1} cells during pup interaction in a hostile virgin female (**h1**) and a mother (**h2**).

(i-l) PETHs of Z-scored ΔF/F of BNSTpr^{Esr1} cells aligned to the onset of various behaviors.

(m) Average area under the curve (AUC) of Z-scored ΔF/F during the first pup contact.

(n-o) Mean AUC of Z-scored ΔF/F during various pup-directed behaviors in different groups.

(p) Representative ΔF/F traces of MPOA^{Esr1} cells during pup interaction.

(q-t) PETHs of Z-scored ΔF/F of MPOA^{Esr1} cells aligned to the onset of various pup-directed behaviors.

(u) Mean AUC of Z-scored ΔF/F during the first pup contact.

(v-w) Mean AUC of Z-scored ΔF/F during various pup-directed behaviors in different groups.

All error bars and shades of PETHs: SEM. Solid and dashed lines in PETH plots indicate the onset and offset of behaviors, respectively. (**m**) Two-sided paired t-test. (**u**) RM one-way ANOVA with multiple comparisons test. (**n, o**) Two-way RM ANOVA with multiple comparisons test. (**v, w**) Mixed-effects analysis with multiple comparisons test. *$p < 0.05$; **$p < 0.01$; ***$p < 0.001$; ****$p < 0.0001$. n = 7 (**i-o**) and 5 (**q-w**) mice/group. See Source Data Fig. 5 for detailed values and statistics.

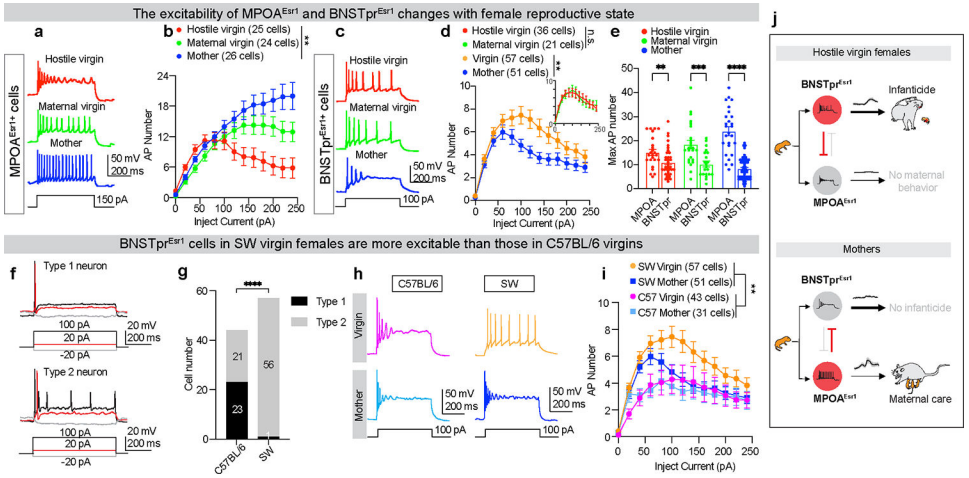

Fig. 6: BNSTpr^{Esr1} and MPOA^{Esr1} cell excitability varies with females' reproductive state and genetic background

(a) Representative recording traces of MPOA^{Esr1} cells.

(b) F-I curves of MPOA^{Esr1} cells from hostile virgin (red, 25 cells/3 mice), maternal virgin (green, 24 cells/3 mice), and lactating (blue, 26 cells/3 mice) SW females.

(c) Representative recording traces of BNSTpr^{Esr1} cells.

(d) F-I curves of BNSTpr^{Esr1} cells from SW virgin females (orange, 57 cells/6 mice) and mothers (blue, 51 cells/9 mice). Inset: F-I curves of BNSTpr^{Esr1} cells from hostile (red, 36 cells/3 mice) and maternal virgin SW females (green, 21 cells/3 mice).

(e) Maximum AP number of MPOA^{Esr1} and BNSTpr^{Esr1} cells from hostile virgin (red, MPOA: 25 cells/3 mice; BNSTpr: 36 cells/3 mice), maternal virgin (green, MPOA: 24 cells/3 mice; BNSTpr: 21 cells/3 mice), and lactating (blue, MPOA: 24 cells/3 mice; BNSTpr: 51 cells/9 mice) SW females with maximally 250 pA injected current.

(f) Representative traces showing spiking patterns of type I and II BNSTpr^{Esr1} cells.

(g) The number of type I and II BNSTpr^{Esr1} cells in C57BL/6 (3 mice) and SW (6 mice) virgin females.

(h) Representative recording traces of type II BNSTpr^{Esr1} cells from C57BL/6 and SW virgin females and mothers.

(i) F-I curves of BNSTpr^{Esr1} cells recorded from C57BL/6 (virgin: 43 cells/3 mice; mother: 31 cells/3 mice) and SW (virgin: 57 cells/6 mice; mother: 51 cells/9 mice) females.

(**j**) A cartoon summary of the antagonism between the infanticide and maternal circuits and theirs changes with reproductive states.

All error bars: ± SEM. (**b, d, i**) Mixed-effects analysis with multiple comparisons test. (**e**) Mann Whitney test (Hostile virgin and Mother) or Unpaired t test (Maternal virgin). (**g**) Fisher's exact test. All tests are two-sided. **p < 0.01, ***p < 0.001, ****p < 0.0001. See Source Data Fig. 6 for detailed values and statistics.